Hindawi
Geofluids
Volume 2022, Article ID 2046267, 26 pages
https://doi.org/10.1155/2022/2046267

Research Article

Applying Imaging Technique to Investigate Effects of Solute Concentrations and Gas Injection Rates on Gas Bubble Generation

Guanxi Yan,[1,2] **Zhixin Cheng**,[1] **Ye Ma**,[1] **Alexander Scheuermann**,[2] **and Ling Li**[2,3,4]

[1]*College of Environmental Sciences and Engineering, Dalian Maritime University, Dalian 116086, China*
[2]*School of Civil Engineering, University of Queensland, St Lucia, QLD, 4072, Australia*
[3]*School of Engineering, Westlake University, Hangzhou 310024, China*
[4]*Institute of Advanced Technology, Westlake Institute for Advanced Study, Hangzhou 310024, China*

Correspondence should be addressed to Guanxi Yan; g.yan@uq.edu.au and Zhixin Cheng; chengzhixin@dlmu.edu.cn

Received 7 September 2022; Accepted 21 September 2022; Published 11 October 2022

Academic Editor: Zhenlong Song

This work investigated the bubble size variation under various aqueous conditions, including saline and surfactant solutions, with different gas injection rates using a commercial bubble analyzer. The results show that salt and surfactant can minimize bubble size with increasing solute concentration, and the surfactant outperforms salt. In addition, the critical coalescence concentrations (CCC) of salt and surfactant could be determined at 20 g/l and 20 mg/l, respectively, over which bubble mean size cannot be further reduced. On the other hand, the gas injection rate, compared to the solute concentration, has minor effects on bubble size variation. Nonetheless, there is a critical coalescence injection rate (CCIR) of 30 ml/min for surfactant solution, over which the standard deviation of the bubble size distribution (BSD) cannot be further increased. In principle, this work improves the accuracy and efficiency of the bubble analyzer. It also presents a sound understanding of two influential factors rather than a single-factor controlling bubble size. Most importantly, it is the first time to observe and propose the concept of CCIR to describe how the gas injection rate influences the standard deviation of BSD. Based on those results and findings, it is able to conclude that bubble size control, whose mechanism has been previously identified as the bubble collision and coalescence rather than the surface tension of water solutions, is actually dominated by not only the solute concentration but also the gas injection rate when a porous air sparger is used to generate bubbles. It is expected that this work could contribute to laboratory modeling bubbly flow in a porous medium in order to bring more insights into the mechanism of soil gas leaking through soil strata.

1. Introduction

The bubbles are gas spherically captured in an aqueous film in a water solution. Bubble size as a significant character for studying two-phase flow has been investigated in a wide range of industries for an extended period. For instance, in marine engineering, the bubbles caused by wave injection significantly escalate gas transfer between the atmosphere and seawater [1–4]. As for mineral engineering, dissolved air flotation is often used to remove individual particles from wastewater and mineral slurries [5–11]. Moreover, microbubble dispersion can improve in situ bioremediation because of its advantages over air sparging, surfactant injection, and bioventing [12–15]. Microbubble dispersion technology has been well studied for various floatation/separation processes and enhanced aeration systems [10, 12, 15, 16].

In addition to the aforementioned applications, the bubbly flow has also drawn research attention from petroleum engineering [17–22] and geoscience [23–28]. For example, Nguyen Hai Le et al. [29] and Nguyen Hai Le et al. [30] most recently reviewed the enhanced oil recovery in sealing highly permeable layers or fractures by injecting carbon dioxide (CO_2) microbubbles as a displacement surrogate. Due to the blocking performance depending on bubble size

distribution (BSD) and stability, Nguyen Hai Le et al. [30] investigated the effects of salt, surfactant, and polymer on the BSD and stability of CO_2 microbubbles. On the other hand, based on the soil gas bubbly flow theory proposed by Etiope and Martinelli [31], Ma et al. [32] studied discrete bubbly flow in water-saturated transparent soil, later followed up by a more comprehensive study by Ma et al. [26]. Furthermore, before modeling multiphase flow in a porous medium [33, 34], it is essential to control and measure bubble size according to the grain size of the transparent soil selected [32, 35–37]. Therefore, bubble size control with the corresponding measurement also facilitates laboratory study of soil gas leakage from saturated subsurface [26, 35, 38] and brings more insights into two-phase flow (gas-water system) in a complex porous medium [33, 34, 39–42].

Several approaches have been developed for bubble size measurement. Rodrigues and Rubio [9] classified them into intrusive and nonintrusive methods. The intrusive methods include electroresistivity [43–46], ultrasound reflection [47–51], and optical techniques [52–58], which inevitably cause instrumented interference on bubble samples. In comparison to those approaches, the imaging technique as a nonintrusive method has been primarily adopted for both academic and industry bubble size measurement due to lower cost and ease of operation [5, 9, 15, 16, 28, 30, 59]. Nevertheless, the densely binding bubbles in the observing chamber bring challenges for image analysis. Usually, the conventional image processing algorithms (e.g., watershed segmentation [60], template matching [61], and shape factor filtering [62]) succeeded in separating and identifying discrete bubbles from bubble clusters for lower bubble density. However, bubble segmentation and identification could fail for higher bubble density, subsequentially leading to overestimating bubble sizes and underestimating sample size. To solve this challenge, Ma et al. [32] established an effective method based on optical physics that shows a linear relationship between the actual diameters of bubbles and bright bubble centroids. As the darker outlines of bubbles separate their bright centroids, conventional image analysis can successfully identify each bright centroid, followed by a correction step to determine the actual bubble size using this linear relationship. The success of this novel method has been well acknowledged by Altheimer et al. [63]. Hence, it is applied to studying bubble size variation under various aqueous environments in this study.

According to Puleo et al. [64], Moruzzi and Reali [65], Shepard et al. [16], and Nguyen Hai Le et al. [30], BSD is dependent on several influential factors: hydraulic pressure in the viewing chamber, the temperature of water solution, solute concentration (surface tension), pH of the aqueous environment, type of injected gas, type of gas bubble generator, gas injection rate, etc. Even though most previous works have investigated multiple factors on BSD, they separately studied and analyzed a single factor of many individually influencing BSD [5, 8, 9, 15, 16, 30, 64, 66, 67]. By far, the significance of combining factors on BSD has not often been investigated.

With an original purpose to control the bubble size for modeling bubbly flow in a porous medium [26, 32, 35], the hydraulic pressure could be assumed hydrostatic for no phreatic surface dynamics, and temperature and pH can be kept constant in the laboratory. Also, Hernandez-Aguilar et al. [68] successfully estimated bubble size variation caused by water solution temperature and hydraulic pressure using an analytical solution derived from the ideal gas law. In addition, earlier studies have investigated the relationship between surface tension and bubble size, concluding that bubble size can be minimized by reducing the surface tension by increasing solute concentration [69]. Later, such a relationship between bubble size and surface tension was experimentally challenged by other recent studies due to the finding of CCC, over which bubble size cannot be minimized with reducing surface tension [9, 70, 71]. Instead of exclusively considering surface tension, the bubble size depends on bubble collision and coalescence, which are governed by the value of solute concentration rather than surface tension. However, whether the solute concentration is the single influential factor dominating the bubble collision and coalescence has not been very often investigated with other potential factors (e.g., gas injection rate for air sparging). Therefore, the research objectives of this study mainly focus on the effects of solute concentrations and gas injection rates on gas bubble generation in water solutions. This work applied a commercial gas bubble analyzer, Anglo Platinum Bubble Sizer, to measure nitrogen gas bubbles generated by a specific gas sparger in various aqueous environments with different gas injection rates. The selection of water solutions included deionized water, saline, and surfactant solutions in several concentrations, each of which was subject to multiple gas injection rates. In principle, this work upgraded the commercial bubble size analyzer in terms of hardware and software. Also, it provides a sound understanding of two influential factors for controlling bubble size rather than a single factor. It is expected that this work could potentially contribute to exploring laboratory modeling bubbly flow in a porous medium in order to improve understanding of the mechanism of soil gas leaking through soil strata.

2. Methodology

2.1. Experimental Setup and Specification. This work selected an industrial bubble size analyzer, Anglo Platinum Bubble Sizer® (manufactured by Stone Three® in South Africa, provided by Julius Kruttschnitt Mineral Research Centre (JKMRC), University of Queensland (UQ), https://jktech.com.au/products/testing-equipment), to capture images of nitrogen gas (N_2) bubble floating through water solutions. Figure 1(a) shows the side view of the experimental setup. Figure 1(b) illustrates that this experimental setup consists of an N_2 gas cylinder, a mass flow controller, a gas sparger, the Anglo Platinum Bubble Sizer, and a digital camera. The entire measuring process can be described in the following steps:

(1) The stored gas was pressurized into the mass flow controller to generate gas bubbles through the sparger at a regulated gas injection rate

(a)

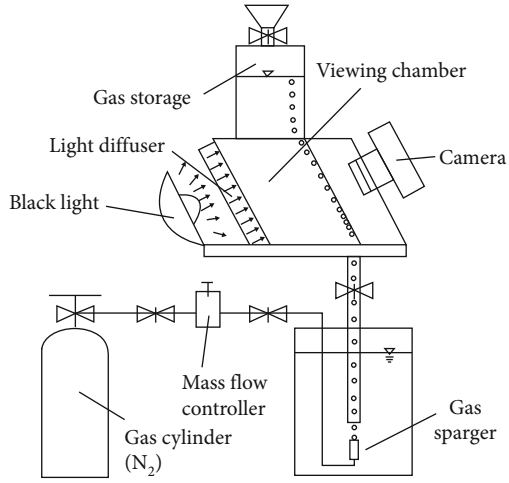

(b)

Figure 1: The experimental setup of bubble size measurement in various water solutions: (a) the side view of Anglo Platinum Bubble Sizer and (b) an illustration of the testing system with bubble sizer.

(2) The gas bubbles, driven by the buoyancy force, floated upward to the viewing chamber through a sampling tube and then glided through the inclined viewing window (13.5° to the vertical axis) in order to form a plane of bubbles with minor overlaps

(3) A digital camera could capture the bubble images within this viewing window, and those bubbles finally reached up to the gas storage at the top of the bubble analyzer

Additionally, it should be noted that before carrying out the test, all aqueous environmental conditions throughout

(a) (b)

Figure 2: The instrument specification: (a) mass flow controller (Brooks® 4800 Series LOI) for regulating the gas injection rate and (b) porous gas sparger (SIKA-R3 AX) selected for the bubble generation.

the entire testing system should be consistent. After meticulously preconfiguring each water solution in the container, the water solution should be filled into the bubble size analyzer. Once the apparatus was completely saturated with the selected solution, the valve at the top should be closed to stop drainage, followed by opening the valve at the bottom. The standard filling procedure provided by JKMRC at UQ was strictly followed.

The gas source is compressed N_2 gas of 200 kPa in a steel cylinder. A mass flow controller was utilized to control the gas injection rates (Brooks® 4800 Series LOI), as shown in Figure 2(a). The mass flow controller could regulate the gas injection rate from 1 ml/min to 50 ml/min with a precision of ±0.01 ml/min. The gas sparger (SIKA-R3 AX) in Figure 2(b) was manufactured by GKN Sinter Metals Filters GmbH. Puleo et al. [64] introduced this product in a study of bubble generation. It is a sintered stainless nozzle with effective pore sizes of 3 μm (see Figure 2(b)), $\Phi d_1 = 10.5$ mm, $\Phi d_2 = 17.5$ mm, $l_1 = 45$ mm, and $l_2 = 11$ mm. A homogeneous LED backlight, powered by a rechargeable battery, was applied to illuminate the viewing chamber through a light diffuser mounted on the back. This setup selected two digital cameras. The original camera appended to this bubble analyzer was Canon Powershot A570 IS (7.1 megapixels CCD sensor and 4x optical zoom with optical image stabilizer). This camera can only measure bubble sizes over 300 μm because of its relatively low resolution. Therefore, the original camera was replaced by another camera, Canon EOS Kiss ×4 SLR (Canon-fabricated single-plate 18 megapixels CMOS sensor, ISO-3200, focal length (50 mm) and *F*-stop value (f/14)), in order to capture bubble images with bubble sizes less than 300 μm. Both cameras captured the same microstage meter of 1000 μm to transform the single-pixel to actual size. As a result, the pixel-size calibrations for Canon Powershot A570 IS and Canon EOS Kiss ×4 SLR are 54.64 μm/pixel and 5.38 μm/pixel separately. It should be noted that the microstage meter has a precision of ±10 μm. Hence, with only 1% of the microstage meter length, the inaccuracy caused by this is negligible.

2.2. Experimental Biases and Precision. A few factors could cause the measurement uncertainties of the bubble size for this experimental setup: bubble contact angle (liquid surface tension), bubble coalescence (gas dissolution in solutions with gas solubility), and bubble volume affected by hydraulic pressure and solution temperature in the viewing chamber. Anfruns [72] studied gas bubbles cut off by the observing window made of glass, concluding that such a bubble-glass

contact causes about 2% bias compared to the actual bubble size, which is insignificant. Marrucci [73] found that bubble coalescence increases with testing time. The N_2 with low dissolubility was chosen to control the gas dissolution. Although the biases result from pressure and temperature related to the testing conditions, an analytical solution derived by Hernandez-Aguilar et al. [68] could correct them. It is in the form of the ideal gas law:

$$\frac{P_{\text{atm}}V}{T} = \frac{P_{\text{i}}V_i}{T_i} \Rightarrow \frac{P_{\text{atm}}}{T}\frac{\pi D^3}{6} = \frac{P_{\text{i}}}{T_i}\frac{\pi {D_i}^3}{6}, \quad (1)$$

where P_{i} is the gas pressure inside gas bubbles ($P_{\text{i}} - P_{\text{o}} = \sigma/R_i$, where P_{o} is hydraulic pressure outside bubble; σ is surface tension and $R_i = D_i/2$ is bubble radius); $V_i = \pi {D_i}^3/6$ is the volume of spherical gas bubbles; D_i is the diameter of spherical bubbles; T_i is the absolute temperature ($273^\circ\text{K} + T_c$, $T_c = 22 \pm 1$ $^\circ$C for water solutions measured by a thermometer in this work); P_{atm} is the atmospheric pressure; $V = \pi D^3/6$ is the volume of spherical gas bubbles for the standard condition (15°C and the atmosphere pressure); D is the diameter of spherical bubbles for the standard condition; and T is the absolute temperature for the standard condition. Equation (1) can also determine the bubble size for different temperatures of water solutions and hydraulic pressures.

Besides, the water solutions expelled from the bubble size analyzer by the injected gas could cause a potential bias in the bubble size measurement. With more solution discharged out, the water level in the container increased, leading to a higher ambient hydraulic pressure around the gas sparger. However, this drainage process only raises concerns of potential bias if the discharged volume is sufficient to increase the water level in the container significantly. In this work, with a container diameter of 28 cm, the water level increase could be controlled to <0.65 cm for injecting gas for 10 min at the highest injection rate of 40 ml/min. Based on Equation (1), a water level increase of <0.65 cm could be seen as a quasi-steady-state flow condition, resulting in negligible underestimations of bubble size. In addition, the bubble rising velocity could also be another influential factor changing the bubble shape under highly hydrodynamic conditions [15]. However, the perfectly spherical shape observed in Figure 3 shows that such an issue is negligible. Also, as this apparatus has no functionality of measuring flow velocity, the effects of water/gas flow velocities were unable to be studied and are beyond the scope of this current work.

2.3. Water Solutions and Gas Injection Rates. There are three selections of water solutions: deionized water, sodium chloride (NaCl), and sodium dodecyl sulphate (SDS) surfactant ($CH_3(CH_2)_{11}SO_4Na$) solutions in various solute concentrations. Salt has been one of the most popular solutes to control bubble size in mineral flotation [74]. The effect of SDS surfactant concentration has also been investigated by Nguyen Hai Le et al. [30] to promote enhanced oil recovery from hydrocarbon reservoirs. Also, both solutes were available in our laboratory. Hence, those water solutions were chosen in consideration of reducing cost for further experiments in discrete bubbly flow in transparent soil. The NaCl concentrations were 10 g/l, 20 g/l, and 30 g/l, corresponding to 10–30 ppt (parts per thousand for saline water). The SDS surfactant concentrations were 0.5 mg/l, 1 mg/l, 5 mg/l, 10 mg/l, 20 mg/l, and 30 mg/l. An electrical scale with a precision of ±0.0001 g (±0.01% for a gram and ±10% for a milligram) was used to measure the dry solute in weight. A measuring cylinder having a precision of ±1 ml (±0.1% for a liter) was used to determine the volume of a water solution. In addition, five different gas injection rates were applied by adjusting the mass flow controller, including 5 ml/min, 10 ml/min, 20 ml/min, 30 ml/min, and 40 ml/min. The mass flow controller could regulate the gas injection rate from 1 ml/min to 50 ml/min with a precision of ±0.01 ml/min. The experimental operating conditions have been summarized in Table 1.

The low-resolution camera captured bubble images of deionized water and saline solutions because bubbles generated in those were relatively larger and therefore needed fewer pixels. The high-resolution camera captured bubble images of SDS surfactant solutions because of smaller bubbles in need of more pixels. Forty to sixty images were captured for each water solution corresponding to each gas injection rate. The first and last ten images were removed from image analysis to avoid larger bubbles at the earlier stage and bubble coalescence at the final stage. The sample sizes given by those bubble images ranged from at least 700 for larger bubbles up to 68000 for smaller bubbles. Based on the principle of sample size provided by Burns and Zhang [75], bubble numbers over 170 ensure a confidence level of 96% for the current experimental condition [59]. It is convincible that the sample size should be sufficient with this sampling arrangement.

2.4. Image Processing Method. Introduced by Leifer et al. [76] and Puleo et al. [64], a public domain image analysis software, ImageJ (developed by the US National Institutes of Health, 1997 and freely accessed by https://rsbweb.nih.gov/ij/), was used to measure the bubble sizes from captured images. The standard bubble image analysis can be achieved in several steps: (1) loading photos in ImageJ, (2) binary pictures by a global grayscale value, (3) filling black color into the white centroid of each bubble, (4) screening out noises by all noise-filtering algorithms available in ImageJ, (5) segmenting binding particles by watershed algorithm, and (6) detecting diameter, area, and perimeter of each bubble by the pixel-counting algorithm in ImageJ. However, this processing method has been demonstrated to fail image analysis for densely binding bubbles [12, 59, 61].

As a motivation, Ma et al. [59] proposed a new image analysis procedure to resolve this scenario effectively in the following steps:

(1) Loading the original photo, see Figure 3(a)

(2) Binary the picture, as shown in Figure 3(b)

(3) Inverting binary image after a binary process (bright bubble centroid switched to black particles in Figure 3(c)). This step has an intrinsic advantage

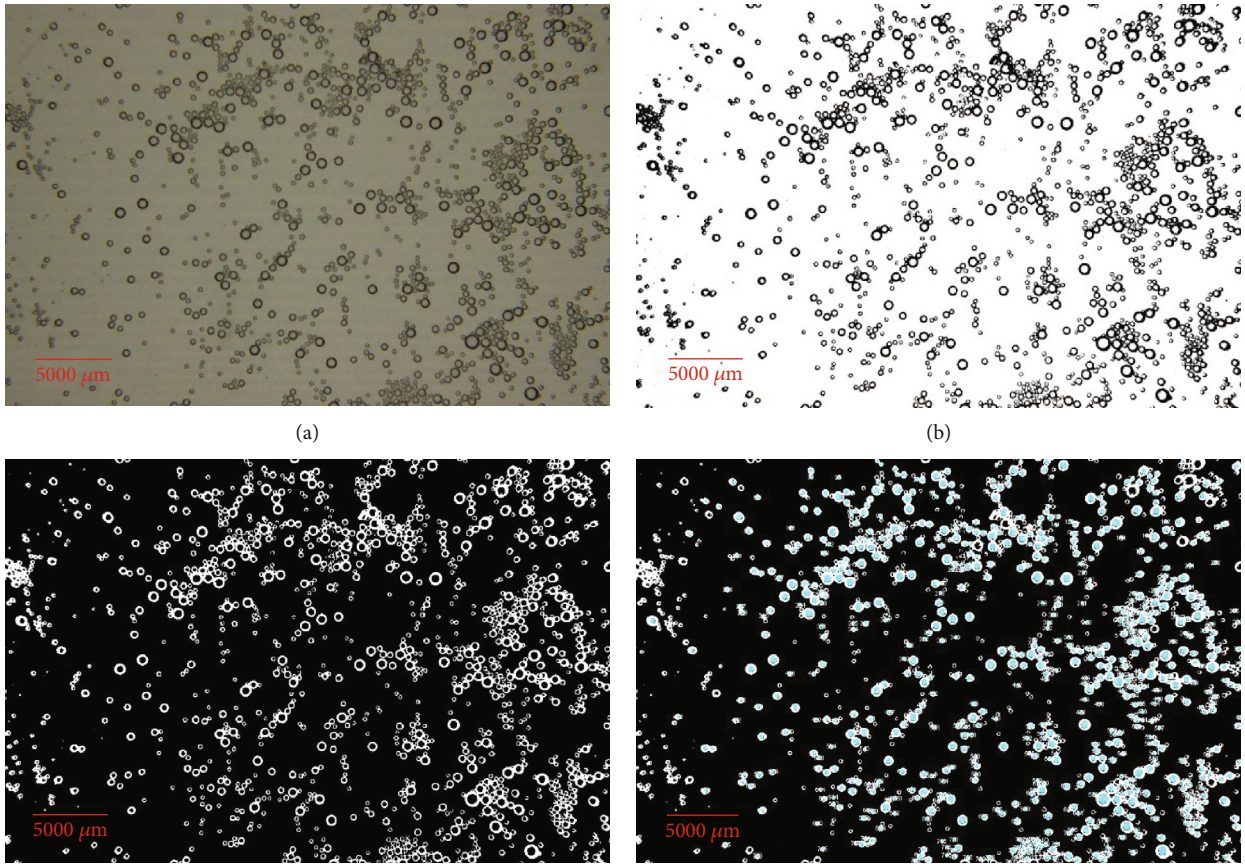

Figure 3: The upgraded image analysis for solving densely binding bubbles: (a) the original image, (b) the binary image, (c) the inverted binary images, and (d) the identification of the bubble bright centroids (highlighted in blue).

Table 1: The selection of the solute concentrations of sodium chloride (NaCl) and sodium dodecyl sulphate (SDS) surfactant ($CH_3(CH_2)_{11}SO_4Na$) and the gas injection rates for each water solution.

NaCl concentration	SDS concentration	Gas injection rate
10 ± 0.0001 g/l	0.5 ± 0.1 mg/l	5 ± 0.01 ml/min
20 ± 0.0001 g/l	1 ± 0.1 mg/l	10 ± 0.01 ml/min
30 ± 0.0001 g/l	5 ± 0.1 mg/l	20 ± 0.01 ml/min
	10 ± 0.1 mg/l	30 ± 0.01 ml/min
	20 ± 0.1 mg/l	40 ± 0.01 ml/min
	30 ± 0.1 mg/l	

that allows a direct measurement of bright bubble centroid by counting the pixels in black. Compared to step (3) in the aforementioned standard method, which detects the entire bubble area after filling black into the white centroid, this method takes advantage of the dark outline of each bubble to separate densely binding bubbles without any segmentations (e.g., the watershed algorithm)

(4) Filtering out none circular bright bubble centroids by a shape factor:

$$C = \frac{4\pi A}{P^2}, \tag{2}$$

where C is the circularity of bubble centroids, adopting 0.7–0.8 in this work. As the sphericity could be well observed in Figures 3 and 4, any particles with $C < 0.7$ have been ruled out as densely binding bubbles, A is the area of bubble centroids, and P is the perimeter of this object, see Figure 3(d). A and P could be given by the pixel-counting algorithm in ImageJ

(5) Counting pixels of circular objects and calculating their inside diameters of bubble bright centroids ID by

$$\mathrm{ID} = 2\sqrt{\frac{A}{\pi}} \tag{3}$$

(6) Determining actual bubble outside diameter of bubble dark outline OD by

$$\mathrm{OD} = k \cdot \mathrm{ID}, \tag{4}$$

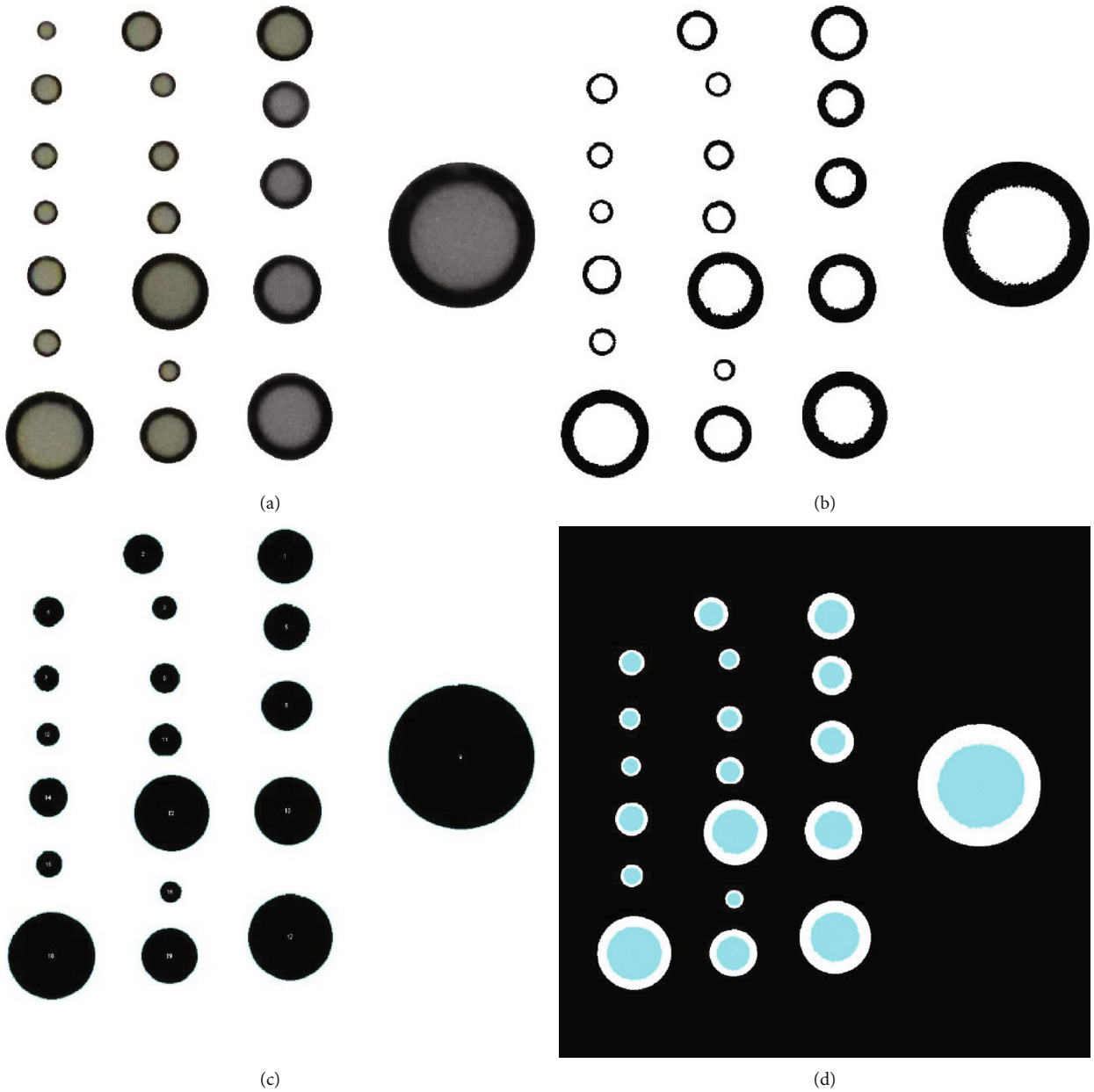

(a) (b) (c) (d)

Figure 4: Continued.

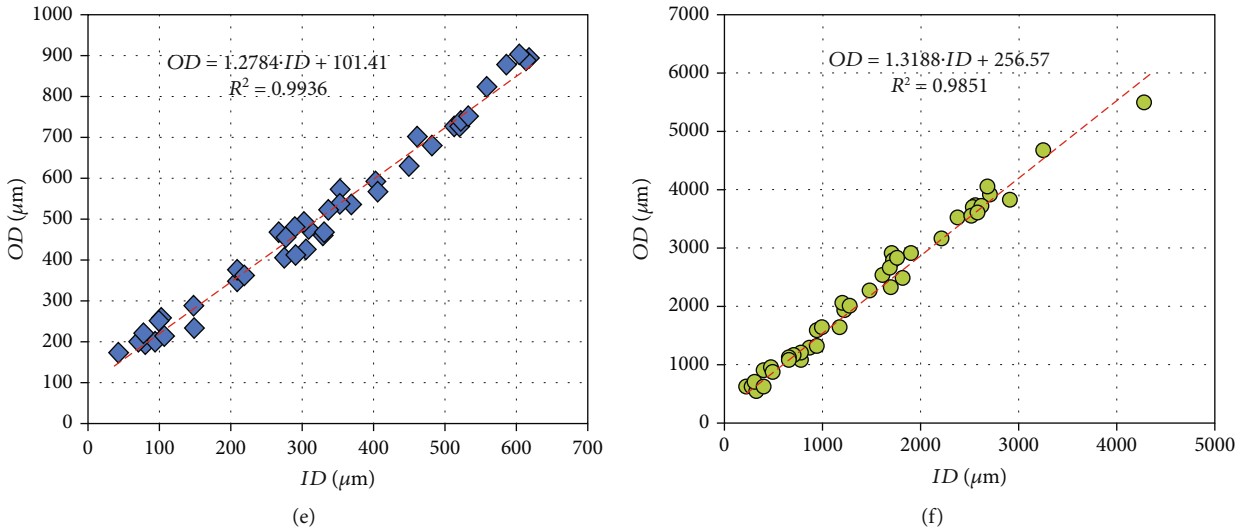

FIGURE 4: The linear regressions to calculate constant k for two cameras: (a) an example of the manual selection of discrete bubbles (e.g., in a smaller sample size for a demo) for determining k of Equation (4) by applying the linear regression, (b) the binarization of the selected bubbles, (c) the measurement of OD using ImageJ by following the standard procedure (targeted bubbles highlighted in black), (d) the measurement of ID by the new procedure (targeted bubble centroids highlighted in cyan), (e) high-resolution camera: Canon EOS Kiss ×4 SLR (18 megapixels), and (f) low-resolution camera: Canon Powershot A570 IS (7.1 megapixels).

where k is a constant between the bright bubble centroids and actual bubble diameters depending on backlight conditions, camera settings, and grayscale value for binary [59]

(7) Statistically analyzing bubble sizes (i.e., OD) estimated by this linear model with the histogram function available in statistic software, such as Excel, MATLAB, and SPSS. The bin width could be adjusted in those selections of software in order to present BSDs in various BSD resolutions in size. In this work, the bin width for the finer group (bubble sizes in 0–1000 μm, bubbles in surfactant solution) was 50 μm, while the bin width for the coarser group (bubble sizes in 1000–5000 μm, bubbles in saline and deionized water) was 100 μm

The advancement of this procedure is to replace segmenting densely binding particles with a linear relation between ID and OD. Bongiovanni et al. [77] have theoretically and mathematically studied this physical phenomenon based on bubble geometrical optics and photometric law. Later, it was experimentally explored and validated by Ma et al. [59], consequently solving densely binding bubbles in images. As for interest in method development, the optical study from Bongiovanni et al. [77] and experimental work from Ma et al. [59] are highly recommended to be followed up in detail. Note that it is only applicable to spherical bubbles by far.

This image analyzing method was applied in this work. Nevertheless, before using this method, two prior linear regressions had to be completed between ID and OD to determine the constant k for two cameras and corresponding image settings. The OD could be determined by applying the aforementioned standard image method to every discrete bubble manually selected from all bubble images (see the instances shown in Figures 4(a)–4(c)). The newly proposed method in steps (1)–(5) could determine the corresponding ID for those selected bubbles (see Figure 4(d)). Note that those manually selected bubbles must cover the full-size range to ensure the validity of k in Equation (4). It has to be done manually because any user has to carefully select the discrete bubbles from a large amount of densely binding ones that cannot be automatically detected by the standard image processing method. According to the sample size investigation from Ma et al. [59], the sample size, ranging from 20 to 200 bubbles, should be sufficient for calibrating this linear relation. Figures 4(e) and 4(f) show the linear regressions for two cameras to determine the constant k values. Both linear regressions achieve $R^2 > 0.985$, and their k values for high- and low-resolution cameras are 1.2784 and 1.3188, respectively. Also, the linear model offsets for both cameras are 101.41 μm and 256.67 μm, which are much over physical length-pixel transformations in 5.38 μm and 54.64 μm for high- and low-resolution cameras, respectively. Both offsets indicate the most miniature objects detected by two cameras and count 19 and 5 pixels, respectively. Theoretically, the smallest detectable bubble/particles could not be over a square dimension of 3 pixels × 3 pixels (i.e., 1 bright pixel surrounded by 4 dark pixels in the shape of a cross in a total of 5 pixels). Human errors in selecting discrete bubbles (see Figure 4(a)) could potentially cause such offsets for the determinations of ID and OD, and the selection of gray scale values for binarizing images (see Figure 4(b)) could be another one. Nevertheless, such a process of bubble selection owned its randomness. A golden principle that should be followed is to preserve the quality and integrity of bubble images as best as possible. In addition, there should be consistency in assigning the gray scale value (a threshold value) from a global scale rather than a single bubble image.

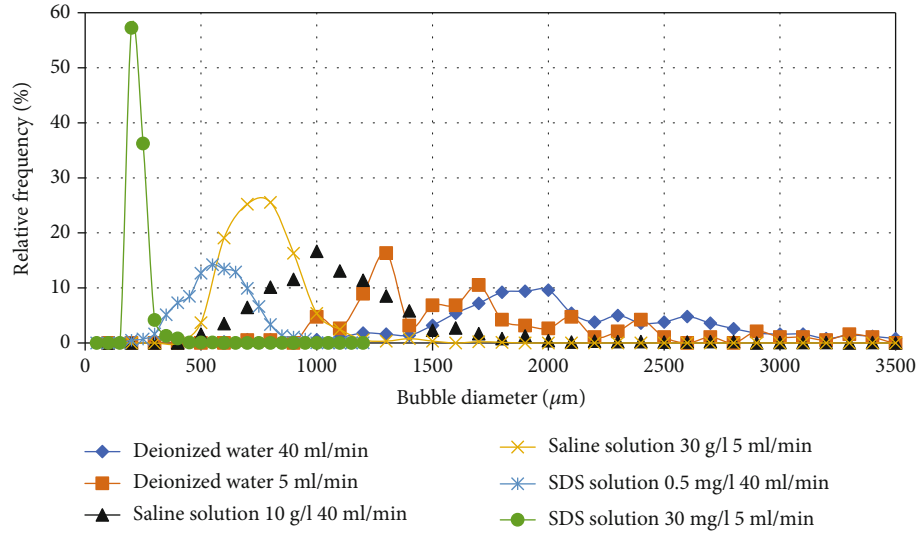

Figure 5: Overall comparison between the solute-added solutions (SDS surfactant and saline water solutions) and deionized water for the highest and lowest gas injection rates.

Ma et al. [59] used the same high-resolution camera for this linear calibration and determined the smallest detectable bubble size of 100 μm, which agrees with the offsets in this work. According to Ma et al. [59], any bubble size less than 100 μm cannot be accurately measured by Canon EOS Kiss ×4 SLR. Actually, this system can still measure bubbles from 54 to 100 μm with an error of <10% because of 5.38 μm/pixel (see Figure 4(e)). Thus, it is expected to measure smaller bubbles by improving image quality and decreasing the pixel-size transformation ratio. Finally, the captured bubble images were processed following the new procedure with these linear regressions.

3. Results and Discussion

3.1. Overall Comparison between the Solute-Added Solutions and Deionized Water. Figure 5 shows the overall comparison between the solute-added solutions (SDS surfactant and saline water solutions) and deionized water without any additives for the highest and lowest gas injection rates (40 ml/min and 5 ml/min). Both SDS surfactant and NaCl can minimize bubble size with increasing solute concentration. Also, the higher the solute concentration and the gas injection rate are, the smaller the span of bubble size distributions (BSD) and the higher the peak of BSD are. In concise, in terms of reducing bubble size, the SDS surfactant solution outperforms the saline solution, and the saline solution outperforms the deionized water. Compared to the range of bubble size for the deionized water within 800–3500 μm, the NaCl solutions can control the range of bubble size within 400–2000 μm, and the SDS surfactant solutions can control the range of bubble size within 150–700 μm. In addition, in terms of the mean value, the NaCl solutions can only control mean size within 700–1200 μm, while the SDS surfactant solutions can control mean size within 190–550 μm.

3.2. Effects of Surfactant Concentrations on Gas Bubble Generation. Figures 6(a)–6(e) present the size distributions of gas bubbles generated in sodium dodecyl sulphate (SDS) surfactant solution in the solute concentration range of 0.5–30 mg/l at gas injection rates of 5 ml/min, 10 ml/min, 20 ml/min, 30 ml/min, and 40 ml/min, respectively. A common among those bubble size distributions (BSD) is that all can be described similarly as unimodal distributions, including both normal and left-skewed distributions. However, for any gas injection rate of five selections, with the concentrations of SDS surfactant increase, the peak of BSD shifts towards a smaller diameter, indicating bubble sizes substantial decrease. Also, their corresponding relative frequency increases from 10%–30% to 40%–60%, indicating more numbers of smaller bubbles generated. Simultaneously, BSD is also narrowed down to a smaller span, indicating a reduction of larger bubbles. Overall, due to adding SDS surfactant into water solutions, the bubble size can be successfully controlled at 100-1000 μm.

In order to more straightforwardly illustrate the statistical variation of BSD with surfactant concentration, the linear mean bubble size and standard deviation of BSD are separately shown in Figures 6(f) and 6(g). Note that the Sauter mean diameter is unnecessary here because the bubble sphericity was preserved well, as the previously mentioned circularity was set over 0.7–0.8. According to Figures 6(f), it is apparent that the mean bubble diameter decreases from 500 μm to 200 μm by increasing surfactant concentration from 0.5 mg/l to 30 mg/l. Similar to the previous studies [9, 29, 30, 78–80], this phenomenon is attributable to the behavior of the solute at the gas-liquid interface. As Aldrich and Feng [69] reported, the surface tension could be substantially decreased by increasing surfactant concentrations. Chaphalkar et al. [79] also noted that the increase in surfactant concentration could minimize the surface tension between the gas and fluid, leading to a higher probability of gas bubble breakup and bubble size decrease. After adding up to a

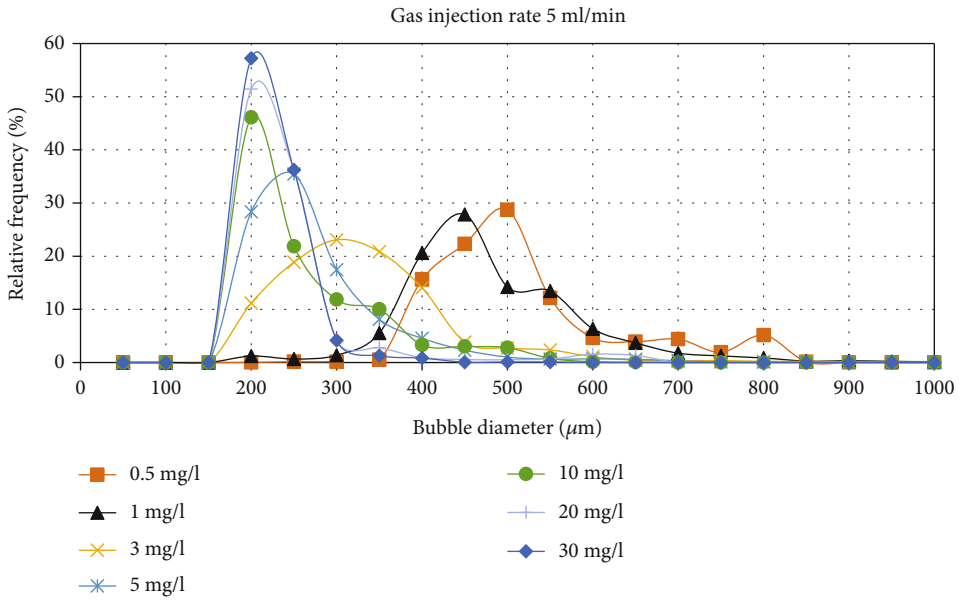

(a)

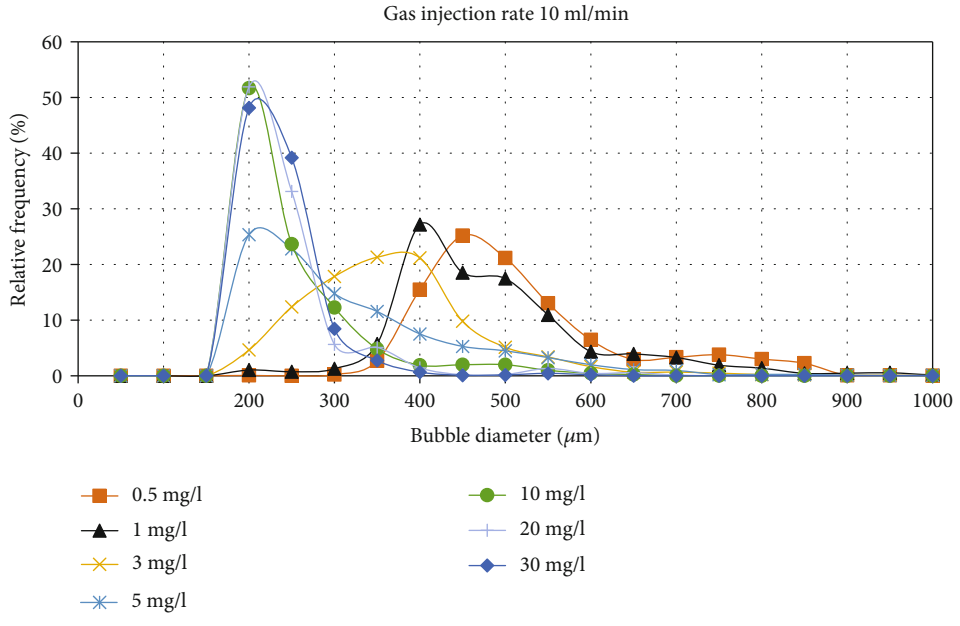

(b)

Figure 6: Continued.

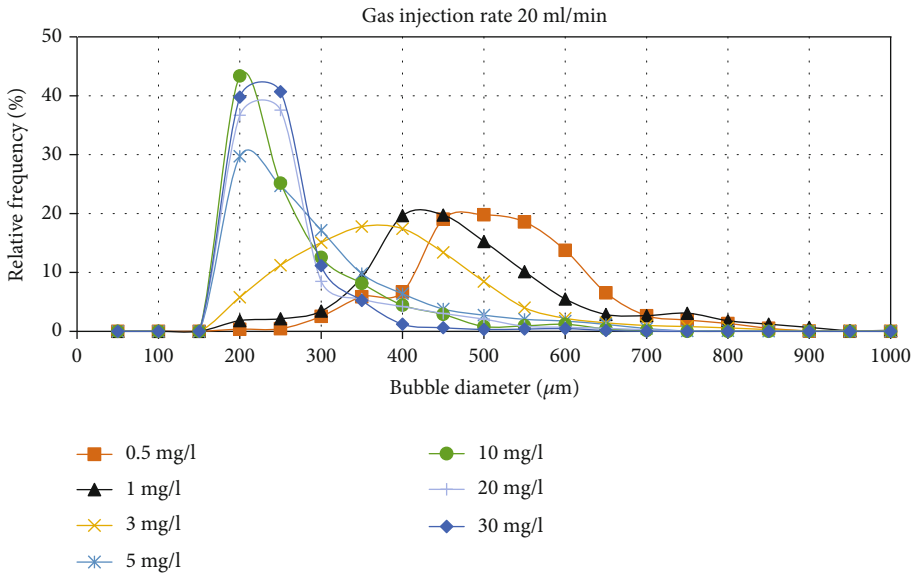

(c)

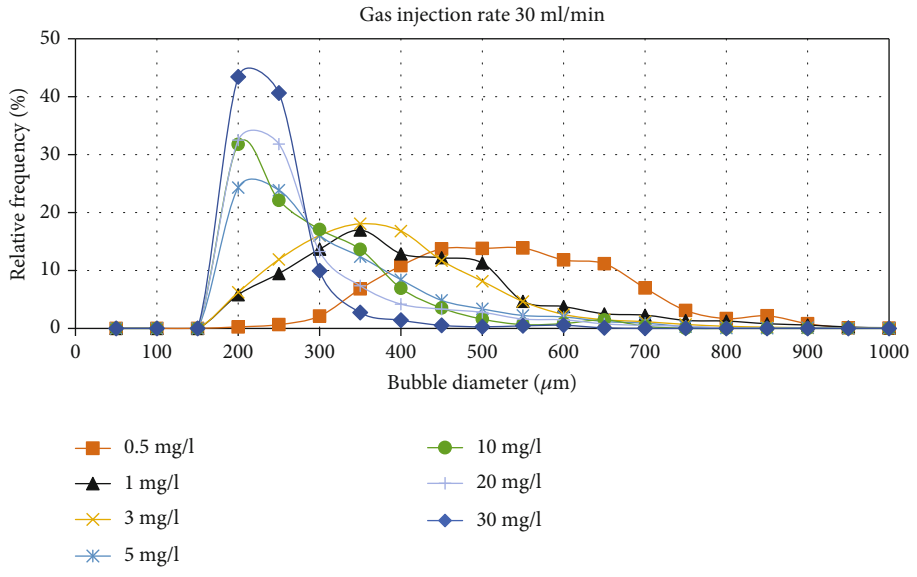

(d)

Figure 6: Continued.

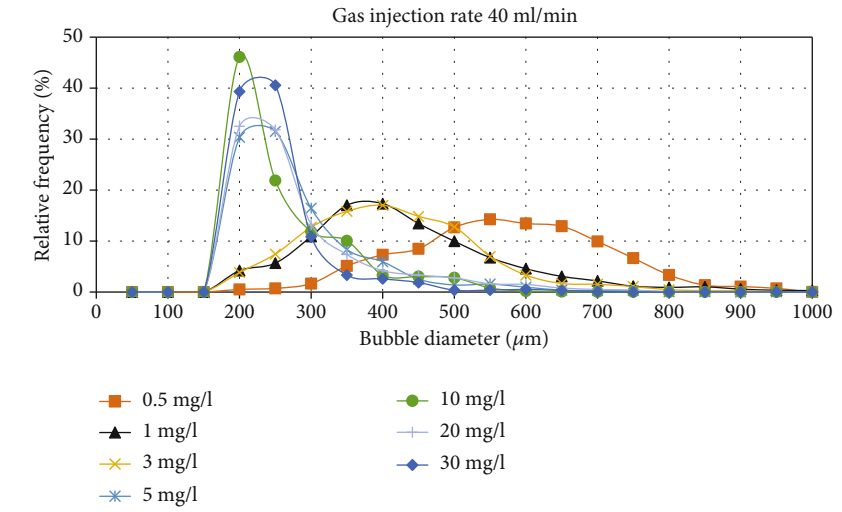

(e)

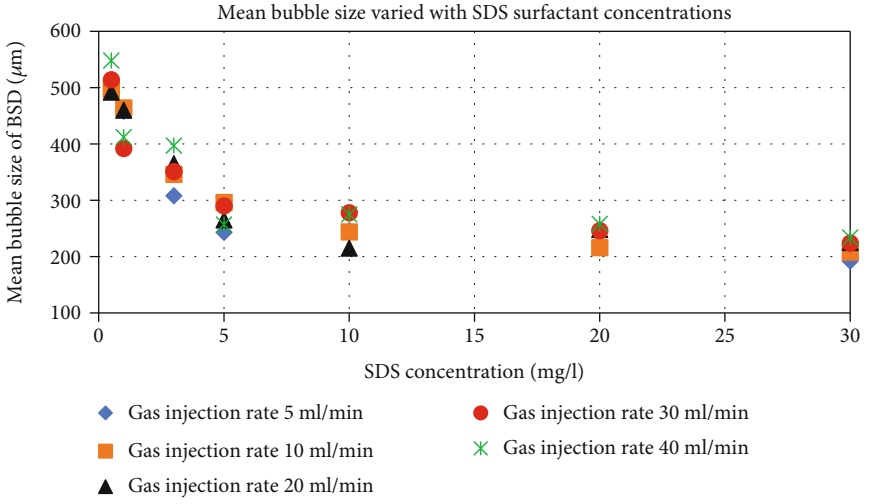

(f)

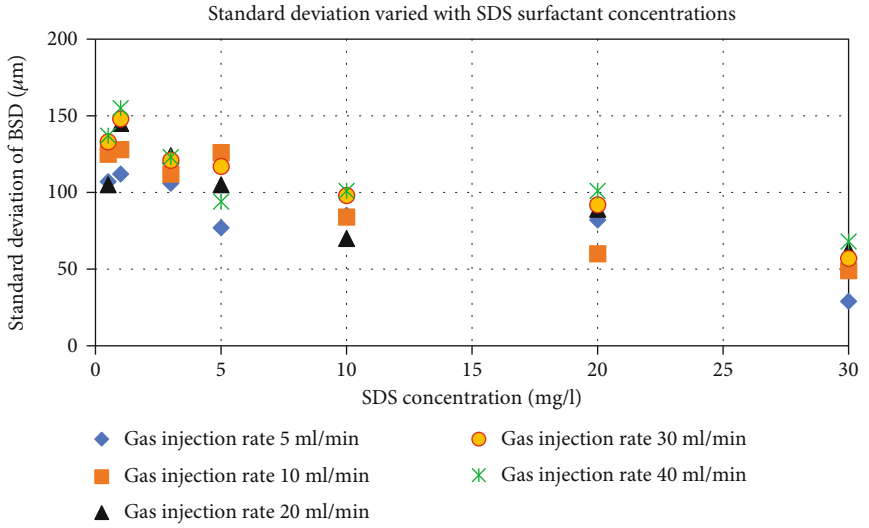

(g)

Figure 6: The effects of sodium dodecyl sulphate (SDS) surfactant concentration on bubble size distribution (BSD) for five different gas injection rates: (a) 5 ml/min, (b) 10 ml/min, (c) 20 ml/min, (d) 30 ml/min, and (e) 40 ml/min. (f) The linear mean bubble size of BSD varied with SDS surfactant concentrations. (g) The standard deviation (STD) of BSD varied with surfactant concentrations.

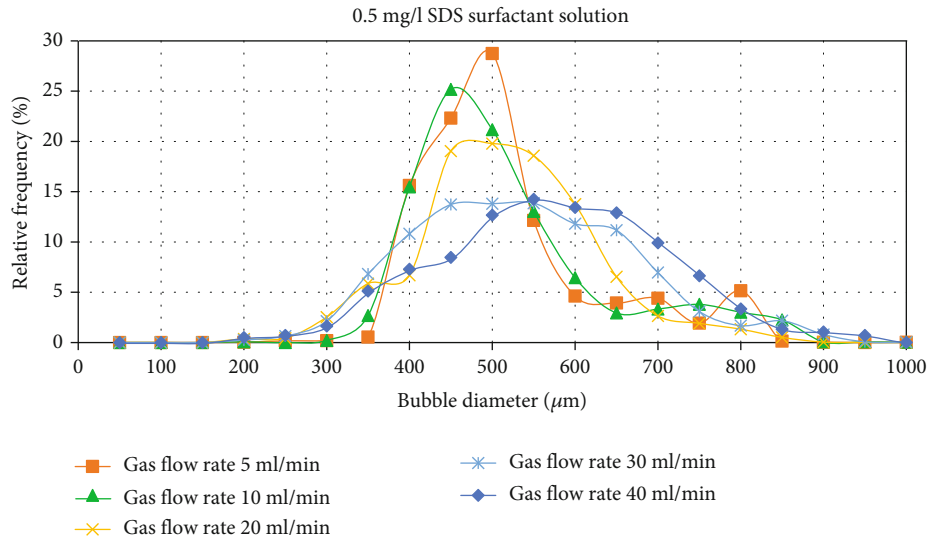

(a)

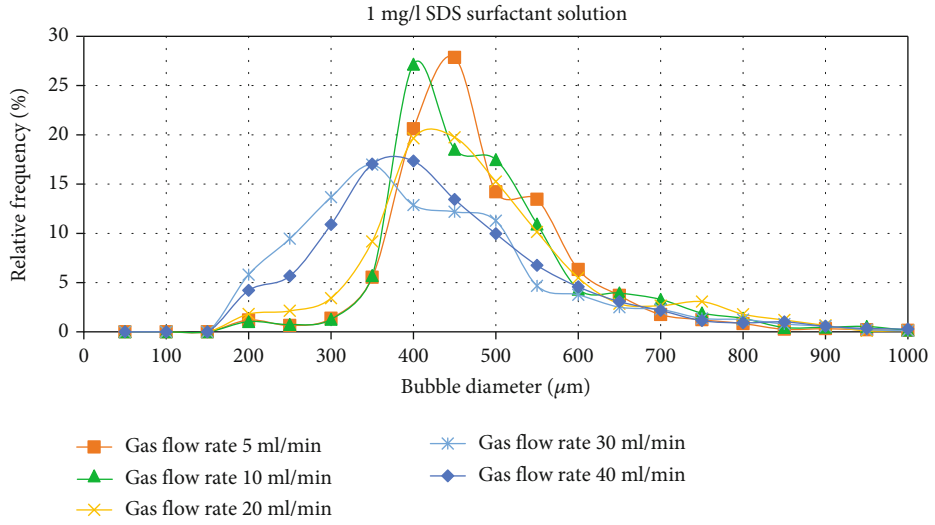

(b)

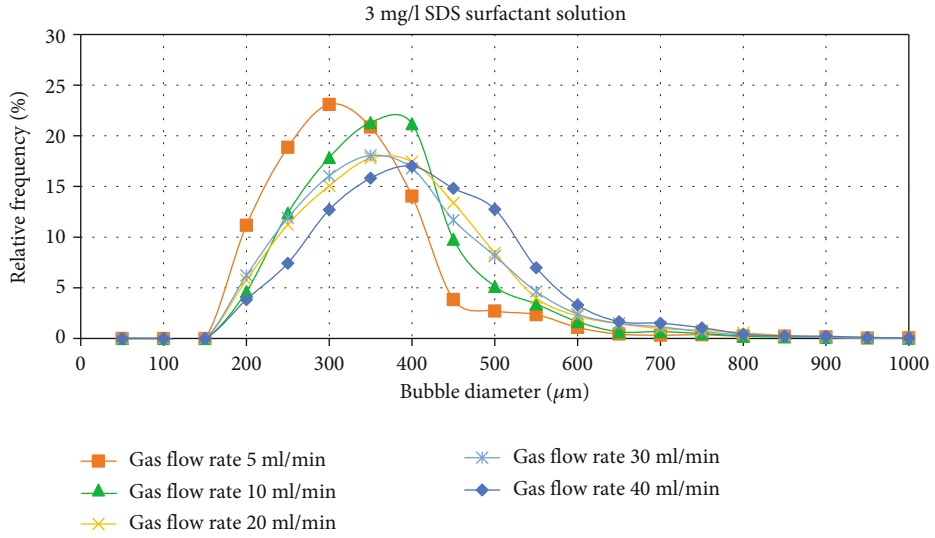

(c)

Figure 7: Continued.

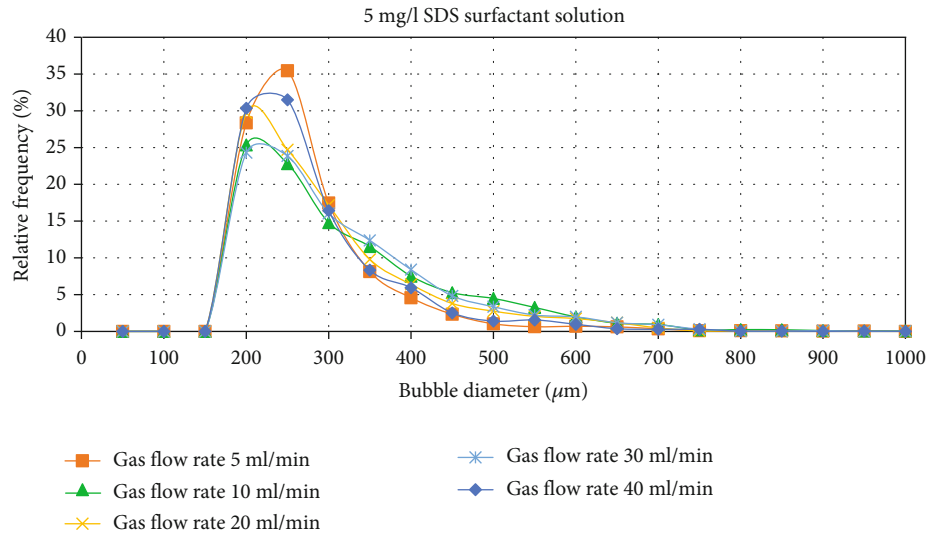

(d)

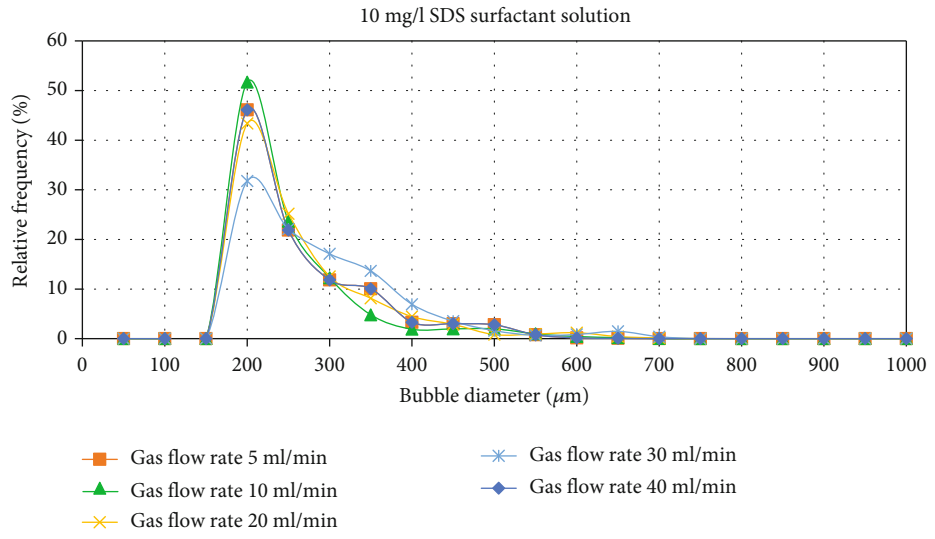

(e)

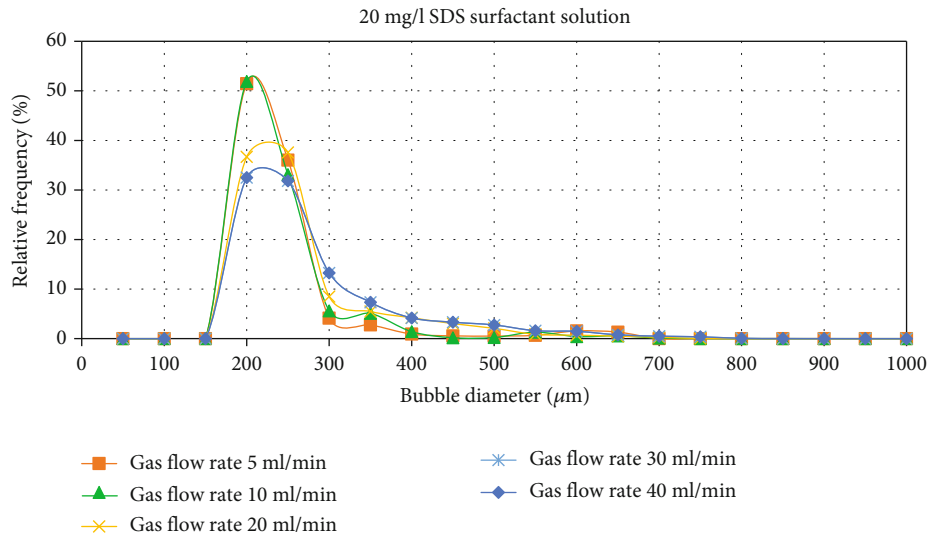

(f)

Figure 7: Continued.

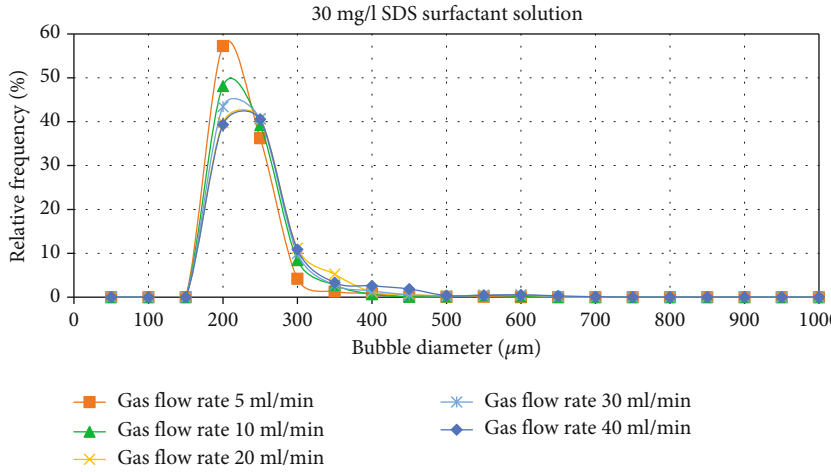

(g)

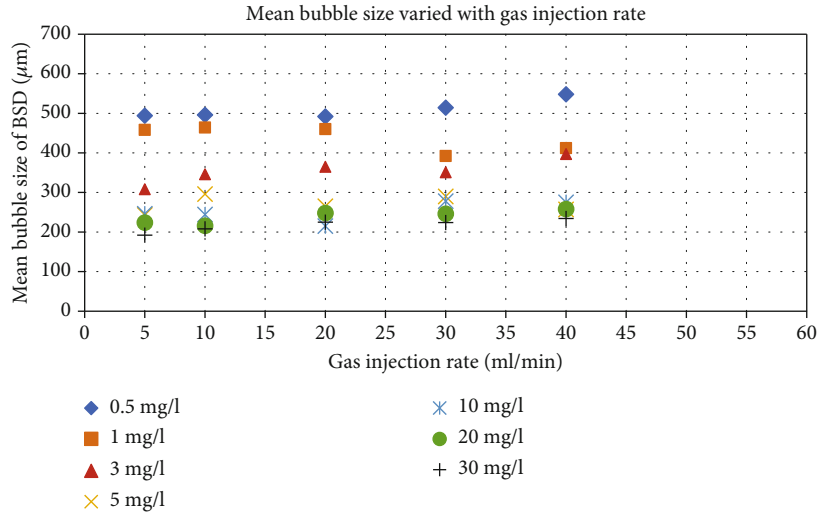

(h)

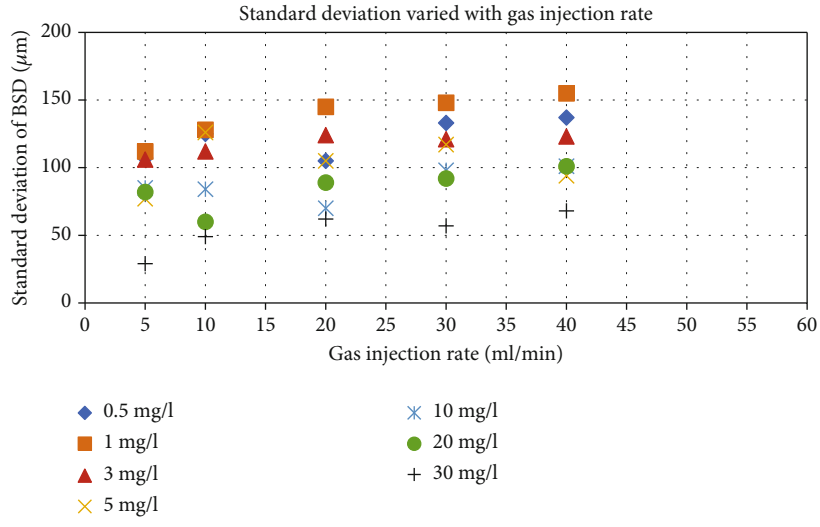

(i)

Figure 7: The effects of gas injection rate on BSD for seven different SDS surfactant concentrations: (a) 0.5 mg/l, (b) 1 mg/l, (c) 3 mg/l, (d) 5 mg/l, (e) 10 mg/l, (f) 20 mg/l, and (g) 30 mg/l. (h) The linear mean bubble size of BSD varied with gas injection rates. (i) The STD of BSD varied with gas injection rates.

critical concentration of 20 mg/l, the mean bubble size gradually reduces compared to a dramatic reduction in bubble size from 0.5 mg/l to 10 mg/l. Figure 6(g) also shows similar features for standard deviation changing with increasing solute concentration. Specifically, the standard deviation of BSD decreases from 150 μm to 50 μm, with concentration rising to 30 mg/l. These results partially agree with Rodrigues and Rubio [9], in which the mean bubble diameter dropped from 700 μm to 250 μm with surfactant concentration increased from 10 mg/l to 30 mg/l. Rodrigues and Rubio [9] also found a critical surfactant concentration of 20 mg/l, over which there was an insignificant reduction of mean bubble size. The reason for observing those minimum mean bubble sizes and standard deviations is due to solute concentration increasing to the critical coalescence concentration (CCC). According to Cho and Laskowski [70, 81], bubble size mainly depends on the solute concentration when the porous gas sparger replaces the single pore gas sparger. Under such conditions, bubble coalescence is the primary mechanism of large bubbles generated at lower solute concentrations [9]. Those coalescences could be prevented if the solute concentration exceeds CCC.

However, these results disagree with Nguyen Hai Le et al. [30] on bubble size controlled by SDS surfactant. In their work, Nguyen Hai Le et al. [30] could control mean bubble sizes to 50–100 μm with standard deviations of 50–80 μm for SDS surfactant added to 1 g/l to 3 g/l, which is not achievable in prior and current studies. This conflicting finding could be due to different gas sources and spargers. For example, Nguyen Hai Le et al. [30] applied carbon dioxide (CO_2) instead of nitrogen gas (N_2) or air (N_2 of 78%) and therefore caused such disagreement. Moreover, Prakash et al. [15] also investigated BSD variation in SDS surfactant solution under highly hydrodynamic conditions (high Reynolds number and large flow velocities). However, due to the different air diffuser and gas injection rates that they applied, there seems less possibility of conducting any comparison against those experimental outcomes. Other studies, including Shepard et al. [16], Alam et al. [5], Pan et al. [8], all studied BSD changing with solute concentrations. Nevertheless, any comparison can still hardly be conducted due to various bubble generating apparatus, different selections of surfactants, fine particles in the fluid, slurry conditions, etc.

3.3. Effects of Gas Injection Rate on Bubbles in Surfactant Solution. Figure 6 merely manifests the BSD, bubble mean sizes, and standard deviations varied with SDS surfactant concentrations. In order to better illustrate the effects of gas injection rates on bubble size, the results from Figures 6(a)–6(e) are rearranged in Figures 7(a)–7(g) to show the BSD varying with gas injection rates for each surfactant concentration. Figures 7(a)–7(g) shows that the gas injection rates can dominate the peak and span of BSD. For lower surfactant concentrations of 0.5 mg/l, 1 g/l, and 3 g/l in Figures 7(a)–7(c), injecting gas at different flow rates can yield BSD without any obvious overlapping and skewing. However, after surfactant concentrations increase over 5 mg/l, all distributions skew to the left and overlap together with minor differences in the peak, as shown in Figures 7(d)–7(g). Specifically, the peak of BSD increases with the decrease in gas injection, indicating smaller bubbles generated at low gas injection rates.

Figures 7(h) and 7(j) present the linear mean bubble size and standard deviation of BSD changing with gas injection rates. Figure 7(h) shows minor effects of gas injection rates on mean bubble sizes for all selections of SDS surfactant concentrations. Nevertheless, Figure 7(j) shows that it indeed dominates the standard deviation. By adjusting the gas injection rate from 5 ml/min to 30 ml/min, the standard deviation can be increased by 20–40 μm. However, further increasing the gas injection rate over this threshold (30 ml/min) cannot enlarge the BSD standard deviations. Hence, SDS surfactant concentration is not a single influential factor exclusively dominating the standard deviation of BSD. Still, higher gas injection rates can also stretch the BSD span, manifested as higher standard deviations. This feature could be attributed to higher possibilities of bubble coalescence resulting from more increased gas injection rates. Therefore, when porous gas sparger is utilized to diffuse gas in water, a critical coalescence injection rate (CCIR), similar to the CCC for solute effects on bubble mean size, should also be considered for injection rate effects on the standard deviation of BSD.

3.4. Effects of Salt Concentrations on Gas Bubble Generation. The effects of sodium chloride (NaCl) concentration on BSD for five different gas injection rates are presented in Figure 8. Figures 8(a)–8(e) shows the largest bubbles generated in deionized water in the form of BSD, spanning from 500 μm to 3000 μm. With the NaCl concentrations increasing from 0 to 30 g/l (0-30 ppt), the BSD skews to the left with a smaller span, indicating mean bubble size and standard deviation decreasing. In addition, the BSD peaks increase by 10–15% when NaCl concentration increases from 0 to 30 g/l. As a result, when adding NaCl into the deionized water over 10 g/l, gas bubble sizes could be controlled in a range between 400 μm and 2000 μm. With NaCl concentration increasing over 10 g/l, all size distributions tend to overlap, with minor differences in the peak. The BSD features are the same as bubble size reduction with increasing surfactant concentration but within different bubble size ranges.

The mean bubble size and standard deviation versus NaCl concentrations are separately shown in Figures 8(f) and 8(g) to illustrate bubble size reduction with increasing NaCl concentrations. It is evident that both mean bubble size and standard deviation monotonically decrease with increasing NaCl concentration. As same as the bubble size reduction by adding more surfactant, the increase in NaCl concentration also leads to a decrease in surface tension, subsequentially resulting in a bubble size reduction [9, 30, 74, 79, 82]. But there is a difference in critical NaCl concentrations for mean size and standard deviation. After adding up to 10 g/l, the mean bubble size could be reduced by approximately 1000 μm. Any further increase in NaCl concentration cannot significantly minimize the mean bubble size. However, as for increasing NaCl concentration from 10 g/l to 20 g/l, the standard deviation can be further decreased by 100–300 μm. When NaCl concentration

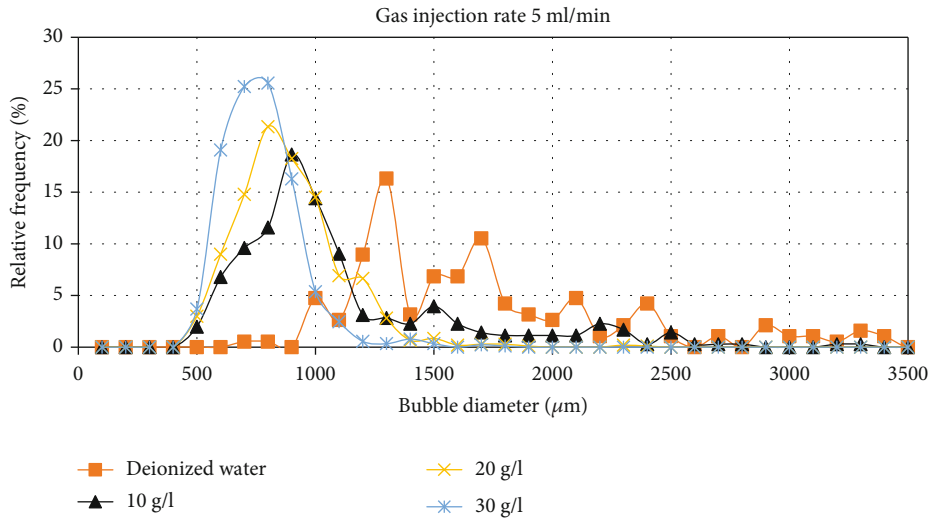

(a)

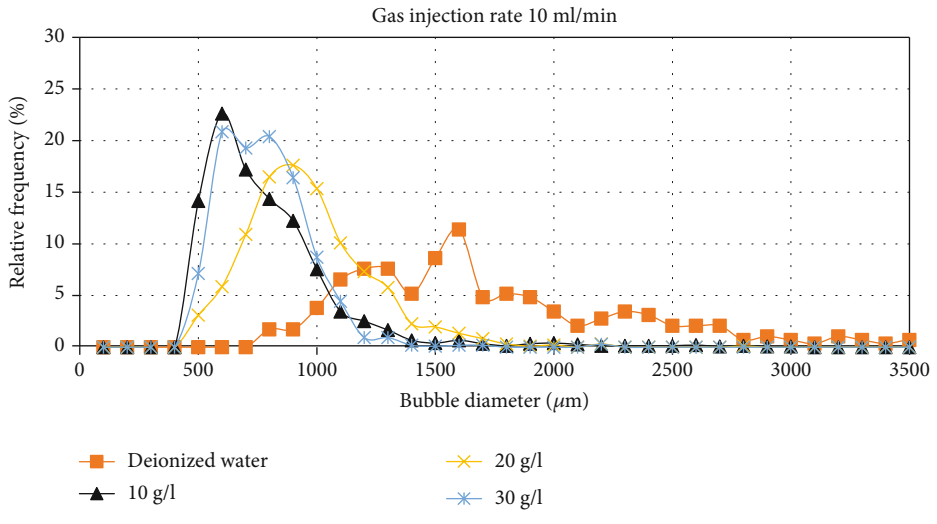

(b)

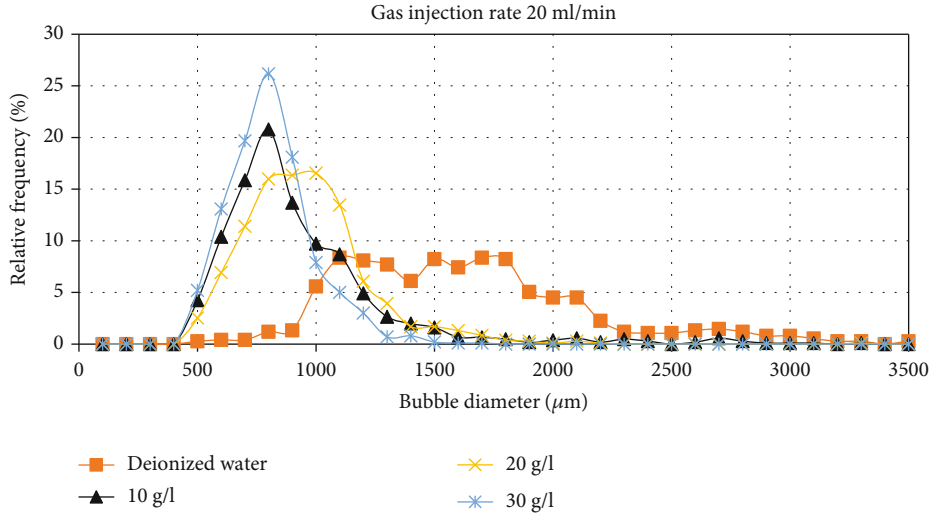

(c)

Figure 8: Continued.

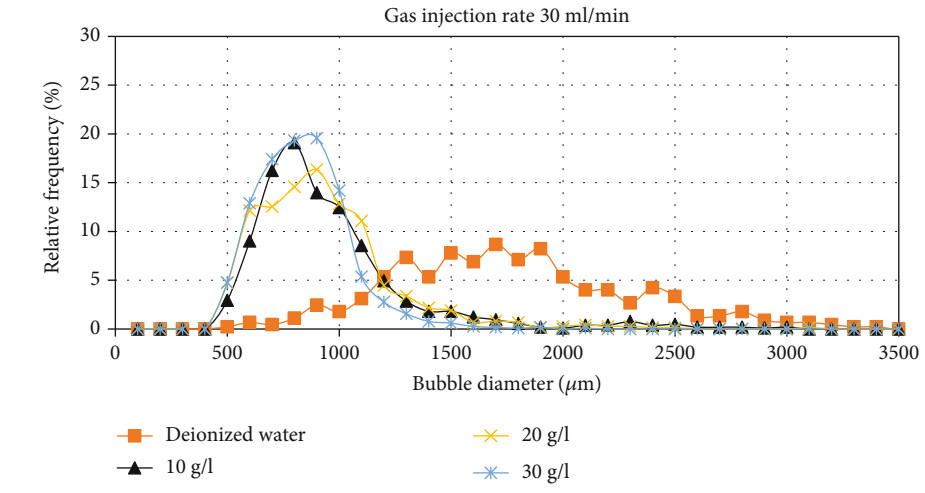

(d)

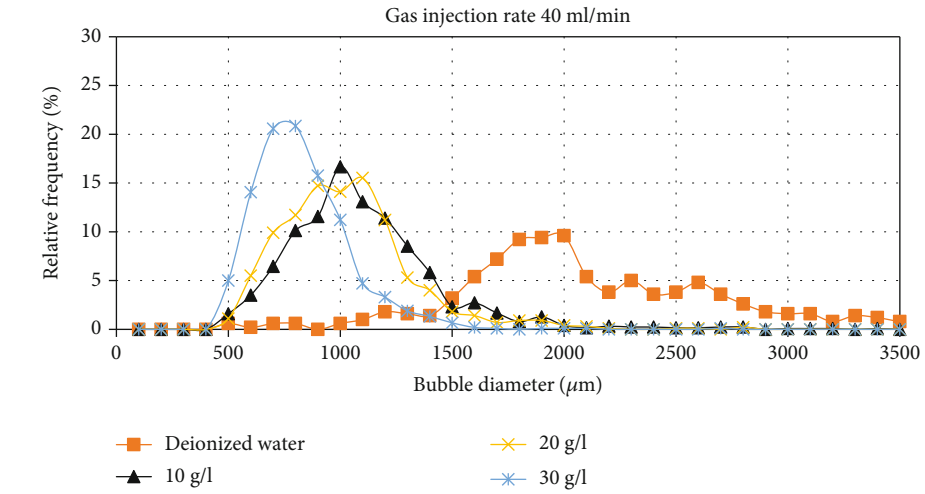

(e)

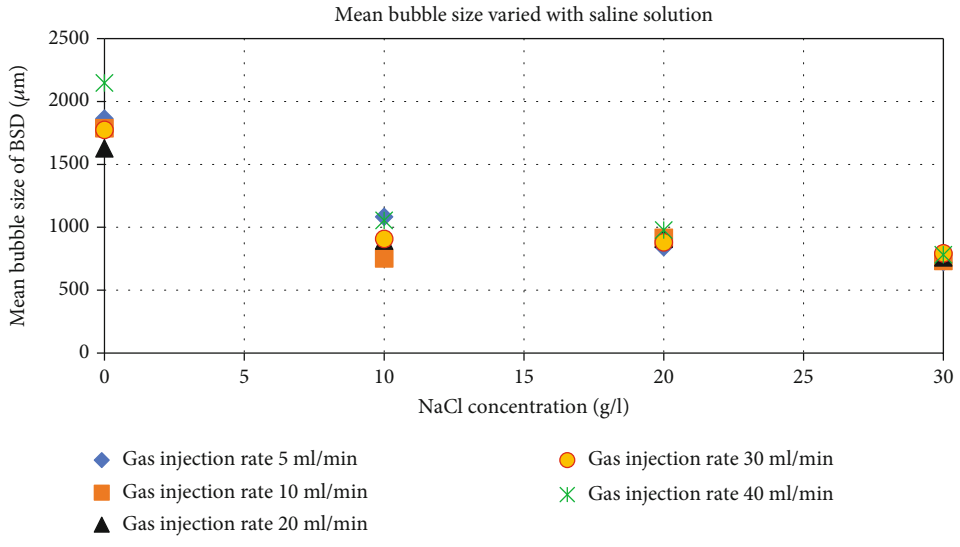

(f)

Figure 8: Continued.

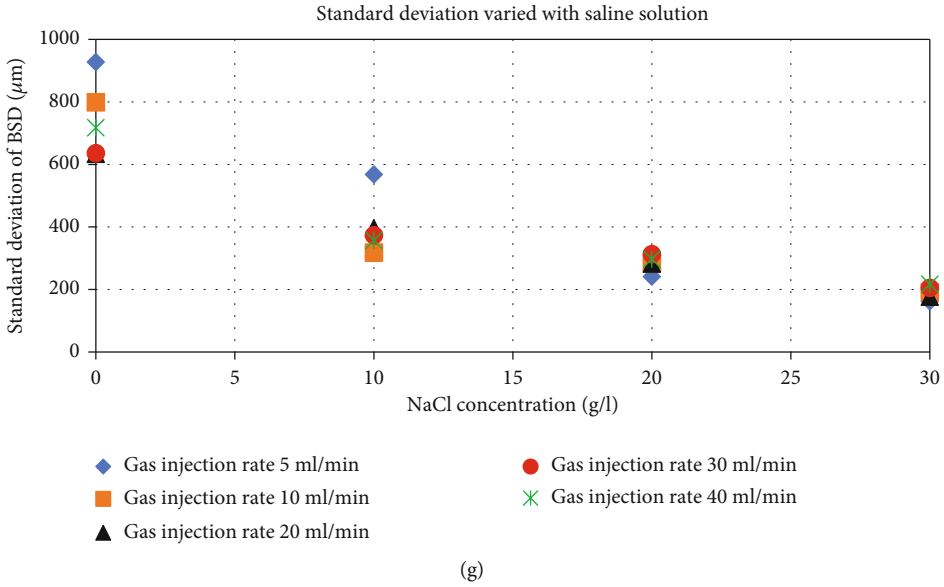

FIGURE 8: The effects of sodium chloride (NaCl) concentration on bubble size distribution (BSD) for five different gas injection rates: (a) 5 ml/min, (b) 10 ml/min, (c) 20 ml/min, (d) 30 ml/min, and (e) 40 ml/min. (f) The mean bubble size varied with NaCl concentrations and (g) the STD varied with NaCl concentrations.

reaches 20–30 g/l, there is no significant decrement of standard deviation (<100 μm). Overall, the CCC of NaCl for mean bubble size could be identified at 20 g/l, although the original definition of CCC only refers to mean bubble size.

Compared to the SDS surfactant solutions that can control mean bubble size within 190–550 μm (see Figures 6(f) and 7(h)), NaCl solutions can only control mean bubble size within 700–1200 μm (see Figures 8(f) and 9(e)). Moreover, the lowest SDS surfactant concentration of 0.5 mg/l is even more efficient than the highest NaCl concentration of 30 g/l in reducing bubble size. Such a comparison also manifests that SDS surfactants reduce the surface tension of water solution more than NaCl. Those findings highly agree with previous studies comparing different surfactants against salt [74, 82].

The selection of those two solutes depends on using purposes. For instance, when laboratory modeling bubbly flows through a porous medium without gas trapping, the SDS surfactant in high concentrations is recommended prior [26, 32]. Instead, the deionized and saline solution should be used if research focuses on bubbly flow in a porous medium with gas trapping. On the other hand, SDS surfactants are applicable to mineral processing in the flotation cell if an air sparger in much finer pore sizes or other bubble generating technique is used. Many mineral processing works have covered bubble sizes ranging from microbubbles to millimeter-bubbles [5, 8, 9, 52, 74, 83]. The selection among those should be dependent on particle size, which needs to be picked up for industrial interest.

3.5. Effects of Gas Injection Rate on Bubbles in Saline Solution. The effects of gas injection rate on BSD for deionized water and saline solutions are given in Figure 9. Figures 9(a) and 9(b) show that the peaks of BSD shift towards the right, indicating a decrease in bubble size. Also, the peaks of BSD decrease as gas injection rates increase. These features only occur for deionized water and saline solution with NaCl concentrations less than 10 g/l (10 ppt). When NaCl concentrations increase over 20 g/l (20 ppt), the BSD for all five gas injection rates almost overlap. Still, the peaks differ by 5%. This pattern also demonstrates that gas injection rates have minor effects on BSD for NaCl concentrations higher than 20 g/l.

The mean bubble sizes and standard deviations of BSD in Figures 9(a)–9(d) are calculated and depicted against gas injection rates in Figures 9(e) and 9(f). Figure 9(e) shows that gas injection rates have insignificant effects on the mean bubble size for NaCl solutions. In contrast, higher injection rates just slightly increase the mean bubble size for deionized water solution because of the higher probability of bubbles collision and coalescence. Also, the mean bubble size can be reduced by 1000 μm when NaCl concentration rises from 0 to 10 g/l. This phenomenon is similar to the bubble size reduction by increasing the surfactant concentrations. As mentioned above, the gas-liquid interface could be more easily broken up by increasing the solute concentration (e.g., salt), resulting from a decrease in the value of surface tension of the tested water solution [30, 74, 79, 82]. However, it should be noted that such a process can be better quantified by solute concentration and gas injection rate. Because of CCC and CCIR, simply correlating bubble size with surface tension could lead to a misunderstanding of bubble collision and coalescence process, thereby failing to physically and numerically model actual BSD.

On the other hand, the standard deviation varying with the gas injection rate in Figure 9(f) shows more conflicting features. As for deionized water, the standard deviation can be minimized by increasing the gas injection rates. However, this finding somehow disagrees with more bubble coalescence and collision for higher injection rates, as

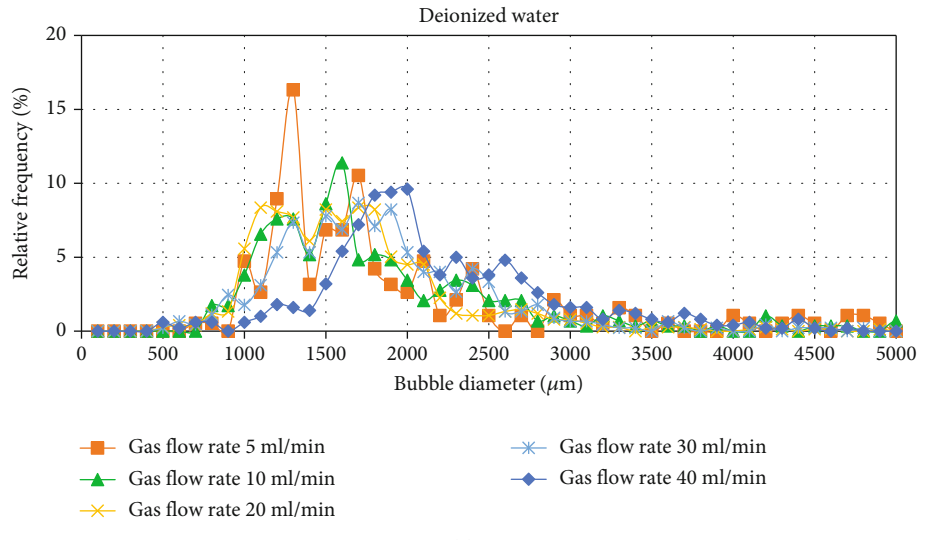

(a)

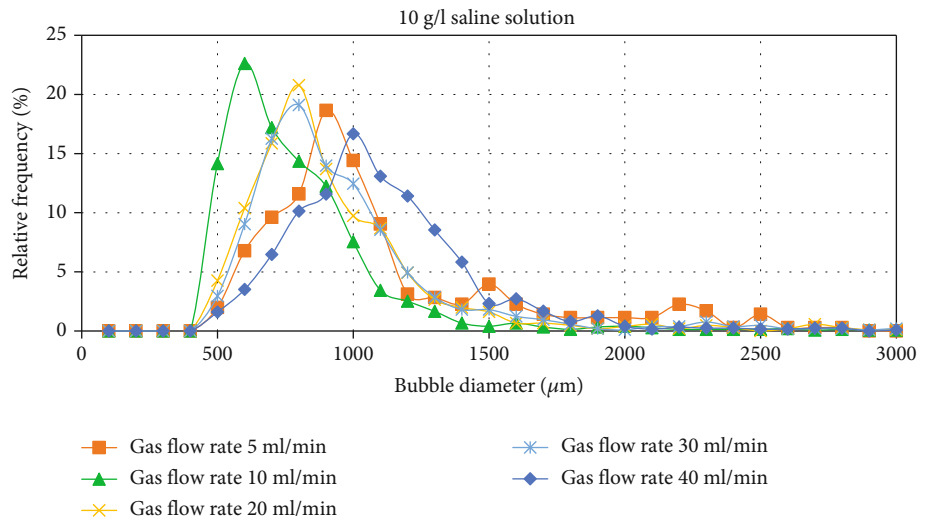

(b)

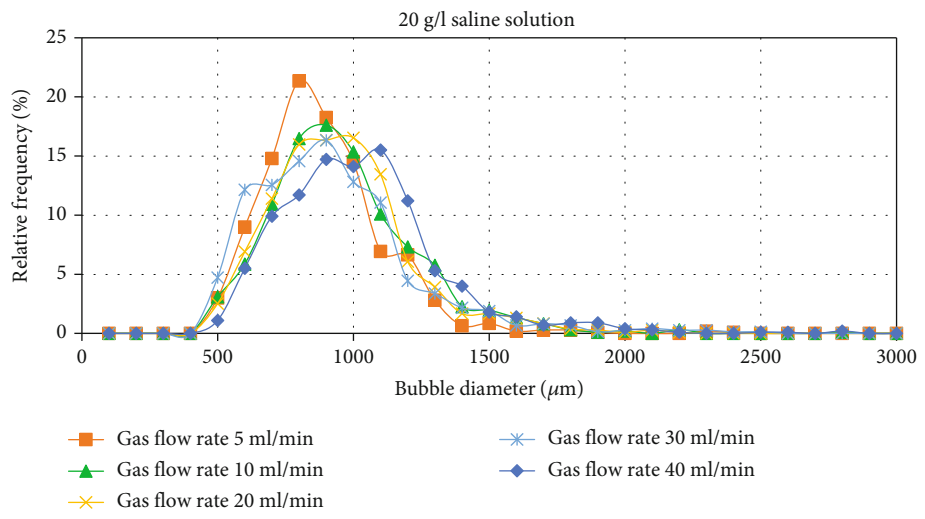

(c)

Figure 9: Continued.

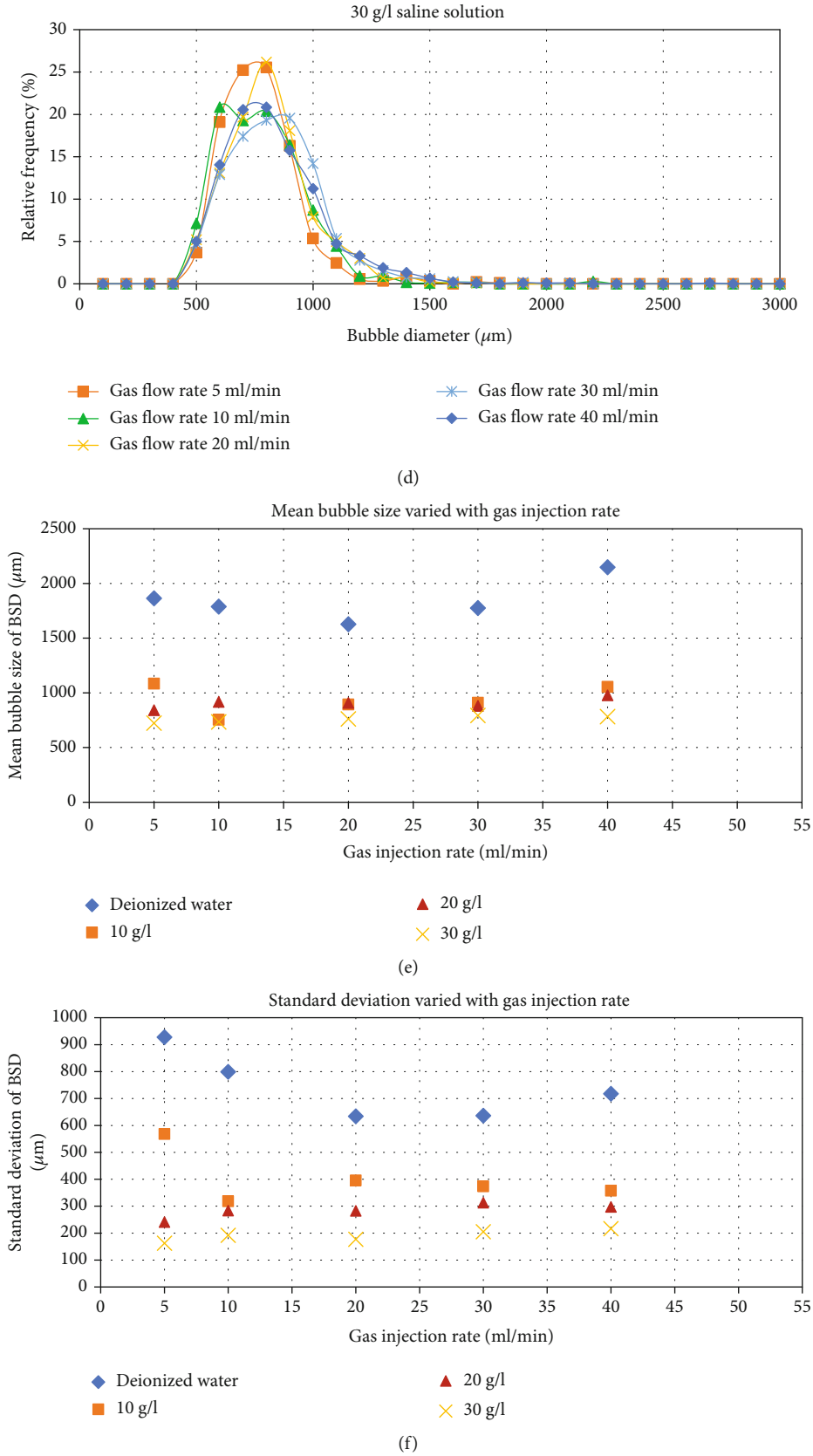

Figure 9: The effects of gas injection rate on BSD for deionized water and saline solutions: (a) 0 g/l deionized water, (b) 10 g/l NaCl solution, (c) 20 g/l NaCl solution, and (d) 30 g/l NaCl solution, (0–30 ppt). (e) The mean bubble size varied with gas injection rates. (f) The STD varied with gas injection rates.

demonstrated in Figure 7(i). Moreover, the standard deviations are not significantly influenced by gas injection rates for NaCl solutions. The physical reasons for such conflicting findings are still unknown and quite debatable. Therefore, it still requires further investigation regarding measuring accuracy for large imperfectly spherical bubbles, the sufficiency of sampling large bubbles, image quality, etc.

4. Conclusions

This work investigates the effects of solute concentrations and gas injection rates on bubble size distribution (BSD). A commercial bubble analyzer, developed based on imaging techniques, was applied to measure gas bubble sizes. The gas bubbles were generated by injecting nitrogen gas through a sintered metal nozzle with five different gas injection rates. The aqueous environments of gas bubbles include deionized water, sodium chloride (NaCl), and sodium dodecyl sulphate (SDS) surfactant solutions in several solute concentrations. Compared to most prior studies separately investigating and analyzing a single influential factor of many on gas bubble size variation, this work explores a combination of two influential factors on BSD.

As the appended camera and standard image analysis failed to determine BSD under the condition of densely binding bubbles, this bubble measuring system was improved by incorporating a high-resolution camera with a newly developed image processing procedure. The original imaging setup can only measure gas bubbles larger than 300 μm for a small number of bubble clusters. With the high-resolution camera, this commercial bubble analyzer can be utilized to measure bubbles down to 100 μm. In addition, compared to the conventional image analysis conducting segmenting algorithms, the new method applied a robust and straightforward linear equation in optical physics to successfully determine the BSD of densely binding bubbles.

Based on the experimental outcomes provided by this measuring system, conclusions can be drawn in the following:

(1) Both SDS surfactant and NaCl can minimize bubble size with increasing solute concentration, and the surfactant outperforms salt. NaCl solutions can only control mean size within 700–1200 μm, while the SDS surfactant solutions can control mean size within 190–550 μm

(2) For the SDS surfactant solution, the mean bubble size and standard deviation of each BSD can be monotonically decreased by increasing SDS surfactant concentrations. There is a critical coalescence concentration (CCC) of 20 mg/l, over which the mean size and standard deviation cannot be significantly minimized by adding more SDS surfactant. The gas injection rates, compared to solute concentrations, have insignificant effects on mean bubble sizes. On the contrary, the standard deviations can be enlarged by increasing the gas injection rates, manifesting more bubble collision and coalescence for higher injection rates. Also, there is a critical coalescence injection rate (CCIR) at 30 ml/min, over which standard deviation cannot be further increased

(3) For NaCl solutions and deionized water, the mean bubble size and standard deviation of each BSD also monotonically decrease with NaCl concentration increases. A CCC of NaCl could be identified at 20 g/l (20 ppt), over which both mean bubble size and standard deviation cannot be reduced by increasing NaCl concentration. The gas injection rate has minor effects on mean bubble size and standard deviation. Also, the CCIR is not identifiable for standard deviation. Those differ from the phenomenon of more bubble coalescence found for SDS surfactant solutions

(4) Many earlier studies have investigated the relationship between surface tension and bubble size, concluding that bubble size can be minimized by reducing surface tension. Later, such a relationship was experimentally challenged by the finding of CCC, over which bubble size cannot be minimized by reducing surface tension. Instead of exclusively considering surface tension, the bubble size depends on bubble collision and coalescence, which are governed by the value of solute. In this work, a new finding is that not only does the solute concentration dominate the bubble collision and coalescence process but also the gas injection rate becomes another contributor. Although this phenomenon is a complex physical process that demands the multiphase computational fluid dynamics in modeling the gas sparging, still, it can be experimentally quantified by the solute concentration and gas injection rate with two aforementioned critical values (including both CCC and CCIR) in a straightforward manner

In summary, this study introduces a commercial bubble size analyzer, which has been improved in both hardware and software (i.e., equipped with a higher resolution digital camera and an effective image processing procedure to avoid densely binding bubbles). Furthermore, it presents a sound understanding of two influential factors for controlling bubble size rather than a single factor. Most importantly, it is the first time to observe and propose the concept of CCIR for the effects of gas injection rate on the standard deviation of BSD. It is expected that this work could facilitate investigating laboratory modeling bubbly flow in a porous medium in order to shed more light on the mechanism of soil gas leaking through soil strata.

5. Patents

The Anglo Platinum Bubble Sizer® was manufactured by Stone Three® in South Africa and provided by Julius Kruttschnitt Mineral Research Centre (JKMRC), University of Queensland (UQ) (accessible at https://jktech.com.au/products/testing-equipment).

Abbreviations

BSD: Bubble size distribution
CCC: Critical coalescence concentration
CCIR: Critical coalescence injection rate
CO_2: Carbon dioxide
N_2: Nitrogen gas
NaCl: Sodium chloride
SDS: Sodium dodecyl sulphate

Nomenclature

A: Area of a bubble centroid
C: Circularity of a bubble centroid
D: Diameter of spherical bubbles for 20°C and the atmosphere pressure
D_i: Diameter of spherical bubbles
ID: The inside diameter of a bubble centroid
k: A constant between the inside and outside diameters of a bubble
OD: The outside diameter of a bubble outline
P: Perimeter of a bubble centroid
P_{atm}: Atmospheric pressure
P_o: Hydraulic pressure outside gas bubbles
P_i: Gas pressure inside gas bubbles
R_i: Spherical bubble radius
T: Absolute temperature for a condition of 20°C and the atmosphere pressure
T_c: Temperature of water solutions in degree of Celsius
T_i: Absolute temperature of water solutions
V: Volume of spherical gas bubbles for 20°C and the atmosphere pressure
V_i: Volume of spherical gas bubbles
σ: Surface tension of water solution

Data Availability

The data is available on request from the corresponding authors.

Conflicts of Interest

The authors declare no conflict of interest.

Authors' Contributions

Conceptualization was done by G.Y. and Y.M. Methodology was done by G.Y. and Y.M. Software was acquired by G.Y. and Y.M. Validation was performed by G.Y. and Z.C. Formal analysis was performed by G.Y. and Z.C. Investigation was performed by G.Y. and Z.C. Resources were acquired by Y.M. and A.S. Data curation was done by G.Y. and Z.C. Writing—original draft preparation was done by G.Y. and Z.C. Writing—review and editing was done by G.Y. and Z.C. Visualization was done by G.Y. Supervision was done by A.S. and L.L. Project administration was done by A.S. and L.L. Funding acquisition was done by Z.C., Y.M., A.S., and L.L. All authors have read and agreed to the published version of the manuscript.

Acknowledgments

We would also acknowledge the support from the Geotechnical Engineering Centre (GEC) and the supplier of Anglo Platinum Bubble Sizer, Julius Kruttschnitt Mineral Research Centre (JKMRC) of the University of Queensland (UQ), Australia. The authors would like to acknowledge support from the National Key Research and Development Program of China (2021YFB2601100) and Fundamental Research Funds for DMU 3132022168. This study was also supported by the National Natural Science Foundation of China (51909114). In addition, the experiments were funded by the Linkage Project (LP120100662), multiscale two-phase flow in complex coal seam systems, funded by the Australian Research Council and supported by a Queensland Science Fellowship awarded to A. Scheuermann.

References

[1] S. Chen, M. B. Timmons, D. J. Aneshansley, and J. J. Bisogni Jr., "Bubble size distribution in a bubble column applied to aquaculture systems," *Aquacultural Engineering*, vol. 11, no. 4, pp. 267–280, 1992.

[2] C. C. Church, "The effects of an elastic solid surface layer on the radial pulsations of gas bubbles," *The Journal of the Acoustical Society of America*, vol. 97, no. 3, pp. 1510–1521, 1995.

[3] D. Farmer, C. McNeil, and B. Johnson, "Evidence for the importance of bubbles in increasing air-sea gas flux," *Nature*, vol. 361, no. 6413, pp. 620–623, 1993.

[4] B. Würsig, C. Greene Jr., and T. Jefferson, "Development of an air bubble curtain to reduce underwater noise of percussive piling," *Marine Environmental Research*, vol. 49, no. 1, pp. 79–93, 2000.

[5] R. Alam, J. Q. Shang, and A. H. Khan, "Bubble size distribution in a laboratory-scale electroflotation study," *Environmental Monitoring and Assessment*, vol. 189, no. 4, pp. 1–14, 2017.

[6] S. Besbes, M. El Hajem, H. B. Aissia, J. Champagne, and J. Jay, "PIV measurements and Eulerian-Lagrangian simulations of the unsteady gas- liquid flow in a needle sparger rectangular bubble column," *Chemical Engineering Science*, vol. 126, pp. 560–572, 2015.

[7] J. Cai, C. Su, Y. Ma et al., "Role of ammonium sulfate in sulfurization flotation of azurite: Inhibiting the formation of copper sulfide colloid and its mechanism," *International Journal of Mining Science and Technology*, vol. 32, no. 3, pp. 575–584, 2022.

[8] Y. Pan, G. Bournival, and S. Ata, "The role of non-frothing reagents on bubble size and bubble stability," *Minerals Engineering*, vol. 161, p. 106652, 2021.

[9] R. T. Rodrigues and J. Rubio, "New basis for measuring the size distribution of bubbles," *Minerals Engineering*, vol. 16, no. 8, pp. 757–765, 2003.

[10] S. Wang, Q. Xia, and F. Xu, "Investigation of collector mixtures on the flotation dynamics of low-rank coal," *Fuel*, vol. 327, p. 125171, 2022.

[11] H. Zhao, R. Ruan, X. Niu, L. Li, and E. Zhang, "A nanoscale qualitative study on the role of sodium hydrosulfide in oxidized carrollite flotation," *International Journal of Mining Science and Technology*, vol. 31, no. 6, pp. 1085–1093, 2021.

[12] W. Feng, *A Study of Rhamnolipid Microbubble Dispersion for Bioremediation Applications: Dispersion Properties and*

Bacteria/Surfactant/Contaminant Interactions, University of Auckland, New Zealand, 2011.

[13] W. Feng, N. Singhal, and S. Swift, "Drainage mechanism of microbubble dispersion and factors influencing its stability," *Journal of Colloid and Interface Science*, vol. 337, no. 2, pp. 548–554, 2009.

[14] S. Mohagheghian and B. R. Elbing, "Characterization of bubble size distributions within a bubble column," *Fluids*, vol. 3, no. 1, p. 13, 2018.

[15] R. Prakash, S. K. Majumder, and A. Singh, "Bubble size distribution and specific bubble interfacial area in two-phase microstructured dense bubbling bed," *Chemical Engineering Research and Design*, vol. 156, pp. 108–130, 2020.

[16] T. G. Shepard, J. Lee, B. Yan, and P. J. Strykowski, "Parameters affecting bubble formation and size distribution from porous media," *Journal of Fluids Engineering*, vol. 138, no. 3, 2016.

[17] N. Bjorndalen and E. Kuru, "Stability of microbubble based drilling fluids under downhole conditions," in *Canadian International Petroleum Conference*, OnePetro, 2006.

[18] M. A. Natawijaya, Y. Sugai, and F. Anggara, "CO_2 microbubble colloidal gas aphrons for EOR application: the generation using porous filter, diameter size analysis and gas blocking impact on sweep efficiency," *Journal of Petroleum Exploration and Production Technology*, vol. 10, no. 1, pp. 103–113, 2020.

[19] S. Razavi, M. Shahmardan, M. Nazari, and M. Norouzi, "Experimental study of the effects of surfactant material and hydrocarbon agent on foam stability with the approach of enhanced oil recovery," *Colloids and Surfaces A: Physicochemical and Engineering Aspects*, vol. 585, article 124047, 2020.

[20] S. Shi, Y. Wang, S. Bai, M. Ding, and W. Chen, "Migration-plugging properties and plugging mechanism of microfoam," *Journal of Dispersion Science and Technology*, vol. 38, no. 11, pp. 1656–1664, 2017.

[21] S. Shi, Y. Wang, Z. Li, Q. Chen, and Z. Zhao, "Laboratory investigation of the factors impact on bubble size, pore blocking and enhanced oil recovery with aqueous colloidal gas aphron," *Journal of Petroleum Exploration and Production Technology*, vol. 6, no. 3, pp. 409–417, 2016.

[22] S. Shi, Y. Wang, Z. Li, M. Ding, and W. Chen, "Experimental study on stability and improving sweep efficiency with microfoam in heterogeneous porous media," *Journal of Dispersion Science and Technology*, vol. 37, no. 8, pp. 1152–1159, 2016.

[23] M. Y. Corapcioglu, A. Cihan, and M. Drazenovic, "Rise velocity of an air bubble in porous media: theoretical studies," *Water Resources Research*, vol. 40, no. 4, 2004.

[24] X. Li and Y. Yortsos, "Theory of multiple bubble growth in porous media by solute diffusion," *Chemical Engineering Science*, vol. 50, no. 8, pp. 1247–1271, 1995.

[25] T. A. Longe, *Colloidal gas aphrons: Generation, flow characterisation and application in soil and groundwater decontamination*, Virginia Polytechnic Institute and State University, Virginia, USA, 1989.

[26] Y. Ma, X. Z. Kong, A. Scheuermann, S. Galindo-Torres, D. Bringemeier, and L. Li, "Microbubble transport in water-saturated porous media," *Water Resources Research*, vol. 51, no. 6, pp. 4359–4373, 2015.

[27] N. Mahabadi, X. Zheng, T. S. Yun, L. van Paassen, and J. Jang, "Gas bubble migration and trapping in porous media: pore-scale simulation," *Journal of Geophysical Research: Solid Earth*, vol. 123, no. 2, pp. 1060–1071, 2018.

[28] J. Oppenheimer, A. C. Rust, K. V. Cashman, and B. Sandnes, "Gas migration regimes and outgassing in particle-rich suspensions," *Frontiers in Physics*, vol. 3, p. 60, 2015.

[29] N. Nguyen Hai Le, Y. Sugai, and K. Sasaki, "Investigation of stability of CO2 microbubbles—colloidal gas aphrons for enhanced oil recovery using definitive screening design," *Colloids and Interfaces*, vol. 4, no. 2, p. 26, 2020.

[30] N. Nguyen Hai Le, Y. Sugai, R. Nguele, and T. Sreu, "Bubble size distribution and stability of CO_2 microbubbles for enhanced oil recovery: effect of polymer, surfactant and salt concentrations," *Journal of Dispersion Science and Technology*, pp. 1–11, 2021.

[31] G. Etiope and G. Martinelli, "Migration of carrier and trace gases in the geosphere: an overview," *Physics of the Earth and Planetary Interiors*, vol. 129, no. 3-4, pp. 185–204, 2002.

[32] Y. Ma, G. Yan, A. Scheuermann, L. Li, S. Galindo-Torres, and D. Bringemeier, "Discrete microbubbles flow in transparent porous media," in *Unsaturated Soils: Research & Applications*, vol. 2, pp. 1219–1223, CRC Press, NSW, Australia, 2014.

[33] G. Yan, Z. Li, T. Bore, S. A. Galindo Torres, A. Scheuermann, and L. Li, "A lattice Boltzmann exploration of two-phase displacement in 2D porous media under various pressure boundary conditions," *Journal of Rock Mechanics and Geotechnical Engineering*, 2022.

[34] G. Yan, Z. Li, T. Bore, S. A. G. Torres, A. Scheuermann, and L. Li, "Discovery of dynamic two-phase flow in porous media using two-dimensional multiphase lattice Boltzmann simulation," *Energies*, vol. 14, no. 13, p. 4044, 2021.

[35] Y. Ma, G. Yan, and A. Scheuermann, "Discrete bubble flow in granular porous media via multiphase computational fluid dynamic simulation," *Frontiers in Earth Science*, vol. 10, 2022.

[36] G. Yan, Y. Ma, A. Scheuermann, and L. Li, "The hydraulic properties of aquabeads considering Forchheimer flow and local heterogeneity," *Geotechnical Testing Journal*, vol. 45, no. 4, pp. 20210234–20210900, 2022.

[37] G. Yan, H. Shi, Y. Ma, A. Scheuermann, and L. Li, "Intrinsic permeabilities of transparent soil under various aqueous environmental conditions," *Géotechnique Letters*, vol. 12, no. 3, pp. 1–7, 2022.

[38] Y. Ma, X. Z. Kong, C. Zhang, A. Scheuermann, D. Bringemeier, and L. Li, "Quantification of natural CO_2 emission through faults and fracture zones in coal basins," *Geophysical Research Letters*, vol. 48, article e2021GL092693, 2021.

[39] G. Yan, T. Bore, H. Bhuyan, S. Schlaeger, and A. Scheuermann, "The technical challenges for applying unsaturated soil sensors to conduct laboratory-scale seepage experiments," *Sensors*, vol. 22, no. 10, p. 3724, 2022.

[40] G. Yan, T. Bore, Z. Li, S. Schlaeger, A. Scheuermann, and L. Li, "Application of spatial time domain reflectometry for investigating moisture content dynamics in unsaturated loamy sand for gravitational drainage," *Applied Sciences*, vol. 11, no. 7, p. 2994, 2021.

[41] G. Yan, T. Bore, S. Schlaeger, A. Scheuermann, and L. Li, "Investigating scale effects in soil water retention curve via spatial time domain reflectometry," *Journal of Hydrology*, vol. 612, p. 128238, 2022.

[42] G. Yan, Z. Li, S. A. Galindo Torres, A. Scheuermann, and L. Li, "Transient two-phase flow in porous media: a literature review and engineering application in geotechnics," *Geotechnics*, vol. 2, no. 1, pp. 32–90, 2022.

[43] C. Bhondayi and M. Moys, "Measurement of a proxy for froth phase bubble sizes as a function of froth depth in flotation machines part 1. Theoretical development and testing of a new technique," *International Journal of Mineral Processing*, vol. 130, pp. 8–19, 2014.

[44] M. Han, Y. Park, and T. Yu, "Development of a new method of measuring bubble size," *Water Science and Technology: Water Supply*, vol. 2, no. 2, pp. 77–83, 2002.

[45] N. Jamshidi and N. Mostoufi, "Measurement of bubble size distribution in activated sludge bubble column bioreactor," *Biochemical Engineering Journal*, vol. 125, pp. 212–220, 2017.

[46] M. R. Rampure, A. A. Kulkarni, and V. V. Ranade, "Hydrodynamics of bubble column reactors at high gas velocity: experiments and computational fluid dynamics (CFD) simulations," *Industrial & Engineering Chemistry Research*, vol. 46, no. 25, pp. 8431–8447, 2007.

[47] J.-Y. Chapelon, D. Cathignol, A. Gelet, and E. Blanc, *Ultrasound therapy apparatus delivering ultrasound waves having thermal and cavitation effects*, Google Patents, 1997.

[48] X. Chen, M. Hussein, and T. Becker, "Determination of bubble size distribution in gas–liquid two-phase systems via an ultrasound-based method," *Engineering in Life Sciences*, vol. 17, no. 6, pp. 653–663, 2017.

[49] H. J. Park, S. Akasaka, Y. Tasaka, and Y. Murai, "Monitoring of void fraction and bubble size in narrow-channel bubbly-flows using ultrasonic pulses with a super bubble-resonant frequency," *IEEE Sensors Journal*, vol. 21, no. 1, pp. 273–283, 2021.

[50] A. Strybulevych, V. Leroy, A. Shum, H. Koksel, M. Scanlon, and J. Page, "Use of an ultrasonic reflectance technique to examine bubble size changes in dough," in *IOP Conference Series: Materials Science and Engineering*, vol. 42, article 012037, IOP Publishing, 2012.

[51] T. Wang, J. Wang, F. Ren, and Y. Jin, "Application of Doppler ultrasound velocimetry in multiphase flow," *Chemical Engineering Journal*, vol. 92, no. 1-3, pp. 111–122, 2003.

[52] S. Biswal, P. Reddy, and S. Bhaumik, "Bubble size distribution in a flotation column," *The Canadian Journal of Chemical Engineering*, vol. 72, no. 1, pp. 148–152, 1994.

[53] H. J. Couto, D. G. Nunes, R. Neumann, and S. C. França, "Micro-bubble size distribution measurements by laser diffraction technique," *Minerals Engineering*, vol. 22, no. 4, pp. 330–335, 2009.

[54] T. Gaillard, C. Honorez, M. Jumeau, F. Elias, and W. Drenckhan, "A simple technique for the automation of bubble size measurements," *Colloids and Surfaces A: Physicochemical and Engineering Aspects*, vol. 473, pp. 68–74, 2015.

[55] J. Li, P. R. White, B. Roche et al., "Acoustic and optical determination of bubble size distributions - quantification of seabed gas emissions," *International Journal of Greenhouse Gas Control*, vol. 108, p. 103313, 2021.

[56] Y. Mizushima, A. Sakamoto, and T. Saito, "Measurement technique of bubble velocity and diameter in a bubble column via single-tip optical-fiber probing with judgment of the pierced position and angle," *Chemical Engineering Science*, vol. 100, pp. 98–104, 2013.

[57] E. J. Terrill and W. K. Melville, "A broadband acoustic technique for measuring bubble size distributions: laboratory and shallow water measurements," *Journal of Atmospheric and Oceanic Technology*, vol. 17, no. 2, pp. 220–239, 2000.

[58] J. Xue, M. Al-Dahhan, M. Dudukovic, and R. Mudde, "Four-point optical probe for measurement of bubble dynamics: validation of the technique," *Flow Measurement and Instrumentation*, vol. 19, no. 5, pp. 293–300, 2008.

[59] Y. Ma, G. Yan, A. Scheuermann, D. Bringemeier, X.-Z. Kong, and L. Li, "Size distribution measurement for densely binding bubbles via image analysis," *Experiments in Fluids*, vol. 55, no. 12, p. 1860, 2014.

[60] A. Seal, A. Das, and P. Sen, "Watershed: an image segmentation approach," *International Journal of Computer Science and Information Technologies*, vol. 6, pp. 2295–2297, 2015.

[61] S. Miskovic, *An investigation of the gas dispersion properties of mechanical flotation cells: an in-situ approach*, Virginia Polytechnic Institute and State University, Virginia, USA, 2011.

[62] M. Bailey, C. O. Gomez, and J. A. Finch, "Development and application of an image analysis method for wide bubble size distributions," *Minerals Engineering*, vol. 18, no. 12, pp. 1214–1221, 2005.

[63] M. Altheimer, R. Häfeli, C. Wälchli, and P. Rudolf von Rohr, "Shadow imaging in bubbly gas–liquid two-phase flow in porous structures," *Experiments in Fluids*, vol. 56, no. 9, pp. 1–16, 2015.

[64] J. A. Puleo, R. V. Johnson, and T. N. Kooney, "Laboratory air bubble generation of various size distributions," *Review of Scientific Instruments*, vol. 75, no. 11, pp. 4558–4563, 2004.

[65] R. B. Moruzzi and M. A. P. Reali, "Characterization of microbubble size distribution and flow configuration in DAF contact zone by a non-intrusive image analysis system and tracer tests," *Water Science and Technology*, vol. 61, no. 1, pp. 253–262, 2010.

[66] Y. Moriguchi and H. Kato, "Influence of microbubble diameter and distribution on frictional resistance reduction," *Journal of Marine Science and Technology*, vol. 7, no. 2, pp. 79–85, 2002.

[67] T. Shepard, E. Ruud, and H. Kinane, "Wall shear effect on bubble formation in turbulent flows," in *Fluids Engineering Division Summer Meeting*, no. article 55560, 2013American Society of Mechanical Engineers, 2013, V01CT17A010.

[68] J. Hernandez-Aguilar, R. Coleman, C. Gomez, and J. Finch, "A comparison between capillary and imaging techniques for sizing bubbles in flotation systems," *Minerals Engineering*, vol. 17, no. 1, pp. 53–61, 2004.

[69] C. Aldrich and D. Feng, "The effect of mothers on bubble size distributions in flotation pulp phases and surface froths," *Minerals Engineering*, vol. 13, no. 10-11, pp. 1049–1057, 2000.

[70] Y. S. Cho and J. S. Laskowski, "Bubble coalescence and its effect on dynamic foam stability," *The Canadian Journal of Chemical Engineering*, vol. 80, no. 2, pp. 299–305, 2002.

[71] C. Sweet, J. Van Hoogstraten, M. Harris, and J. Laskowski, "The effect of frothers on bubble size and frothability of aqueous solutions," in *Processing of Complex Ores–Proc. 2nd UBC-Mc Gill Int. Symp. Metallurgical Society of CIM*, pp. 235–245, Montreal, 1997.

[72] J. P. Anfruns, *The flotation of small particles*, no. article U416751, 1976England, University of London, Imperial College of Science and Technology, United Kingdom, 1976.

[73] G. Marrucci, "A theory of coalescence," *Chemical Engineering Science*, vol. 24, no. 6, pp. 975–985, 1969.

[74] J. Quinn, W. Kracht, C. Gomez, C. Gagnon, and J. Finch, "Comparing the effect of salts and frother (MIBC) on gas dispersion and froth properties," *Minerals Engineering*, vol. 20, no. 14, pp. 1296–1302, 2007.

[75] S. Burns and M. Zhang, "Digital image analysis to assess microbubble behavior in porous media," *Journal of Computing in Civil Engineering*, vol. 13, no. 1, pp. 43–48, 1999.

[76] I. Leifer, G. De Leeuw, and L. H. Cohen, "Optical measurement of bubbles: system design and application," *Journal of Atmospheric and Oceanic Technology*, vol. 20, no. 9, pp. 1317–1332, 2003.

[77] C. Bongiovanni, J. P. Chevaillier, and J. Fabre, "Sizing of bubbles by incoherent imaging: defocus bias," *Experiments in Fluids*, vol. 23, no. 3, pp. 209–216, 1997.

[78] M. A. Ahmadi, M. Galedarzadeh, and S. R. Shadizadeh, "Colloidal gas aphron drilling fluid properties generated by natural surfactants: experimental investigation," *Journal of Natural Gas Science and Engineering*, vol. 27, pp. 1109–1117, 2015.

[79] P. Chaphalkar, K. Valsaraj, and D. Roy, "A study of the size distribution and stability of colloidal gas aphrons using a particle size analyzer," *Separation Science and Technology*, vol. 28, no. 6, pp. 1287–1302, 1993.

[80] Q. Xu, M. Nakajima, S. Ichikawa et al., "Effects of surfactant and electrolyte concentrations on bubble formation and stabilization," *Journal of Colloid and Interface Science*, vol. 332, no. 1, pp. 208–214, 2009.

[81] Y.-S. Cho and J. Laskowski, "Effect of flotation frothers on bubble size and foam stability," *International Journal of Mineral Processing*, vol. 64, no. 2-3, pp. 69–80, 2002.

[82] W. Kracht and J. Finch, "Bubble break-up and the role of frother and salt," *International Journal of Mineral Processing*, vol. 92, no. 3-4, pp. 153–161, 2009.

[83] R. Grau and K. Heiskanen, "Bubble size distribution in laboratory scale flotation cells," *Minerals Engineering*, vol. 18, no. 12, pp. 1164–1172, 2005.